https://doi.org/10.5194/egusphere-2024-1666
Preprint. Discussion started: 11 June 2024

Impact of short-term atmospheric warming events on the Ice sheet surface and subsurface temperatures of coastal Dronning Maud Land, East Antarctica

Eledath M Gayathri[1,2], Chavarukonam M Laluraj[1], Karathazhiyath Satheesan[3], Kenichi Matsuoka[4], Mahalinganathan Kanthanathan [1] and Meloth Thamban[1]

[1]National Centre for Polar & Ocean Research, Ministry of Earth Sciences, Goa, India

[2]School of Earth, Ocean and Atmospheric Sciences, Goa University, Taleigao Plateau Goa, India

[3]Department of Atmospheric Sciences, School of Marine Sciences Cochin, University of Science and Technology, Cochin, Kerala, 682016, India

[4]Norwegian Polar Institute, Tromsø, Norway

Correspondence to: Eledath M Gayathri (gayathriem@ncpor.res.in)

Abstract. Short-term, episodic atmospheric warming events over Antarctica have received considerable attention for their direct role in establishing record-high temperatures, surface melting, and their indirect impacts via associated high wind speed and precipitation. However, there is limited knowledge of the effect of these warming events on the ice sheet surface and subsurface temperatures, despite their critical role in firn microphysical properties. Using reanalysis dataset ERA5 and ice sheet surface and subsurface temperature records from an ice core-borehole (71.5 °S, 10.25 °E) from coastal Dronning Maud Land (cDML), we examined the air (T2m) warming, subsurface warming, regional and large scale drivers of 70 short term ice sheet surface warming (ISSW) events covering a period 2014-2018. Out of 70 ISSW events, 60 occurred during periods of strong easterly winds with high snow accumulation and the rest during strong southeasterly winds (katabatic) without any precipitation. The former events resulted from increased downward longwave radiation and warmer air above associated with warm air advection from cyclonic intrusions. With an average frequency of 12 events/year, they established the highest ISSW over the region including the maximum warming of ~11 °C raising the ISST from -34 °C to -25 °C (in 9 days) recorded over the period and penetrating deeper in the snowpack (40-125 cm). Here, the T2m showed a minimum warming of 4.4 °C and a maximum of 24.6 °C, leading the ISSW by two days. The latter events were associated with turbulent mixing from strong, dry and anomalously warm winds from the interior. Although the T2m warmed significantly (4.4-15 °C) without any lead/lag, these events showed modest ISSW (2-5 °C) and shallow heat penetration to snowpack (40-60 cm) but resulted in significant sublimation over the region. Our study suggests that the impact of atmospheric warming events on ice sheet surface and subsurface temperatures varies with meteorological conditions. The frequent occurrence of these events might alter the firn's water-retaining capacity, which becomes crucial when surface melting reaches beyond the grounding line in a continued warming scenario. In the future, it is anticipated that their effects will increase as greenhouse gas concentrations rise.

https://doi.org/10.5194/egusphere-2024-1666
Preprint. Discussion started: 11 June 2024

1. Introduction

Short-term atmospheric warming events occur periodically throughout the year over Antarctica, perturbing the daily average near-surface temperature for a brief period. (Argentini et al., 2014). They are associated with strong near-surface winds and often with very high precipitation. High precipitation concurrent with these warming events contributes to about 40% of total annual precipitation across Antarctica, which has significant implications on ice core interpretation (Schlosser et al., 2016; Turner et al., 2019). Bliss et al. (2011) observed rapid sublimation during the occurrence of strong near-surface winds associated with these events. In some instances, these warming events resulted in air temperatures well above freezing recorded over the continent (de Los Milagros Skansi et al., 2017; Bozkurt et al., 2018; González-Herrero et al., 2022) and resulted in widespread surface melting in summer (Zou et al., 2021a, b; Tjernström et al., 2015; Nicolas et al., 2017).

While air temperature and ISST are highly correlated, they differ in magnitude depending on meteorological conditions such as cloud cover and wind speed over the region (Nielsen-Englyst et al., 2019). Presently, there is a limited understanding of the impact of these atmospheric warming events on the Ice Sheet Surface Temperature (ISST), despite its critical role in surface and subsurface processes. At the surface, ISST determines the energy balance, sublimation, and melt rates. Major subsurface processes like refreezing of meltwater, snow metamorphism, and firn densification rely on the ISST (Ligtenberg et al., 2011; Jordan et al., 2008; Trabant and Mayo, 1985). Frequent warming episodes can raise the temperature of snowpack reducing its ability to refreeze the meltwater (Trabant and Mayo, 1985). This has direct effects on the health of the firn layer (Firn Symposium Team et al., 2024), which acts as a buffer against ice sheet mass loss and sea level rise by retaining and refreezing surface meltwater (Noël et al., 2018; van Wessem et al., 2018; Shepherd et al., 2018). For example, increased temperatures increase grain growth rate and size (Spaulding et al., 2011) which affects the pore space available for liquid transport and permeability of the firn layer (Courville et al., 2010; Albert and Shultz, 2002). The largest uncertainty in predicting the state of firn in the future lies in how it behaves with rapid atmospheric warming events (Firn Symposium Team et al., 2024). Therefore, gaining insight into the behaviour of ISST and subsurface temperatures under various atmospheric warming scenarios might be advantageous for monitoring the health of the firn layer in the future.

Previous studies on the drivers of these atmospheric warming events revealed that their meteorological and synoptic conditions varied spatially over Antarctica. In the Pacific sector of West Antarctica, the sudden increase in temperatures and melting has been attributed to the intrusion of warm, moist air (Emanuelsson et al., 2018; Ghiz et al., 2021; Nicolas and Bromwich, 2011; Nicolas et al., 2017). It was found to happen most often during El Niño events (Nicolas et al., 2017). There are several observations of warming events over the West and East Antarctica due to warm air advections (Sinclair, 1981; Wille et al., 2019; Zou et al., 2021a, b). Additionally, warming events over the eastern Antarctic Peninsula and McMurdo Dry Valleys in the Transantarctic Mountains have been linked to episodic mountain foehn winds (Bozkurt et al., 2018; Cape et al., 2015; Speirs et al., 2010; King et al., 2017). Such foehn wind originating from the Antarctic Peninsula (van den Broeke, 2005; Scambos et al., 2000) triggered the collapse of the ice shelves of Larsen A in 1995 (Rott et al., 1996) and Larsen B in 2002 (Scambos et al., 2004). Persistent katabatic winds have also warmed the surface of the Roi Baudouin Ice Shelf in Dronning Maud Land (Lenaerts et al., 2017). The intensity and duration of wind-induced warming depend mainly on the synoptic conditions and topography of the

https://doi.org/10.5194/egusphere-2024-1666
Preprint. Discussion started: 11 June 2024

region (Bromwich et al., 1993; Heinemann, 2000). A warming event over the Amery Ice Shelf in East Antarctica has been reported to be from warm air advection associated with an atmospheric river and strong downslope winds from the interior (Turner et al., 2022). Downslope winds from the interior are generally very cold in contrast to warm maritime air (Hogan, 1997; Vihma et al., 2011). However, in the above warming event, the southerly winds were very warm as a result of a 'recurved foehn wind', where a warm air mass recurved its path upon reaching elevated inland and directed towards the coast with an additional warming from adiabatic compression (Turner et al., 2022). There have been very few studies of this mechanism for producing warm air intrusions in the coastal region. The evolution of the surface temperature in Antarctica is complex due to local and large-scale influences, hence a regional-scale study is required for its holistic understanding.

Numerous studies have delved into understanding the frequency and duration of warming events, examining their spatial and temporal variability continent-wide (Turner et al., 2021; Feron et al., 2021; Speirs et al., 2010; Cape et al., 2015). The intensity and frequency of extreme warming events exhibited opposing trends over the Antarctic Peninsula and coastal East Antarctica, with the former showing an increasing trend and the latter decreasing during the period 1970-2000 (Wei et al., 2019). However, for the subsequent period, the number of extreme events decreased across the entirety of Antarctica, but with different regional trends (Turner et al., 2021). Feron et al. (2021) conducted a model study to predict the frequency and duration of extreme warming events during the summer over the entire Antarctica under two emission scenarios and revealed increasing trends in both parameters by the end of this century. Therefore, understanding the frequency and duration of extreme warming events and their effects on the ice sheet surface remains critical for assessing its stability in the future.

Satellites provide an excellent dataset for ISST with high spatial coverage however they are limited to clear sky conditions. Therefore, to examine the Ice Sheet Surface Warming (ISSW) events under different meteorological conditions throughout the year, a dataset with high temporal coverage is required. In the current study, we examine a new dataset for measurements of ice sheet surface and subsurface temperatures of the region, using six-hourly temperature measurements from an ice core borehole, covering a period from 2014 to 2018. We discuss the elaborate methodology of using thermistor measurements for deriving ISST and ground heat flux for a long period. With simple and relatively inexpensive data retrieval and processing, this dataset could provide the unique observational basis for the validation of satellite and model outputs, and most importantly fill the data gap existing currently over Antarctica.

To understand the firn changes during rapid short-term warming events, a better understanding of the relationship between air temperature, ISST and subsurface temperature is required. The aims of this study are (i) to understand this relation by comparing their extent and timing of warming for different meteorological conditions, (ii) to identify the regional and synoptic drivers that have more impact on ice sheet surface and subsurface and (iii) to examine their frequency and seasonality over the region. For this, we sorted major ISSW events and categorized them based on their meteorological conditions. Later, their corresponding air (T2m) warming, subsurface warming and regional and large-scale drivers, are examined by conducting two case studies. Finally, we looked into their amplitude, frequency and seasonality over the region for the period. One category of ISSW events identified in our study was associated with warm surface southerly winds which are relatively less studied over Antarctica and we conducted the first multi-year study of them over cDML. Finally, we discuss the implications of these warming events over the

https://doi.org/10.5194/egusphere-2024-1666
Preprint. Discussion started: 11 June 2024

region. The results from this study can provide valuable insights for refining firn models and advancing studies on firn microphysics.

2. Data and methodology

2.1 Study Region

The study area is situated in the Atlantic sector of the Southern Ocean (Figure 1a). Dronning Maud Land (DML) covers a large area of East Antarctica, with its 2000 km long coast characterized by extensive ice shelves interspersed with numerous ice rises and rumples that have a key role in the stability of the ice sheet (Matsuoka et al., 2015; Goel et al., 2020). The complex terrain of cDML comprises various surface and subsurface features. During summer, extensive networks of supraglacial lakes and streams are observed over the ice shelves of DML, with surface temperature being one of the key controls (Moussavi et al., 2020; Arthur et al., 2020; Dell et al., 2020; Stokes et al., 2019). The region consists of various other morphological features including blue ice areas, meltwater channels, frozen lakes and crevasses (Chouksey et al., 2021). Subsurface melting was observed beneath a blue ice area in the Jutulgryta area of cDML even at sub-freezing air temperatures as a result of high solar radiation penetration (Liston et al., 1999). Firn cores retrieved from the coastal regions on DML provided evidence of coastal melting through the melt layers identified during the study period (Dey et al., 2022; Kaczmarska et al., 2006). The complex terrain of cDML with such elaborate supraglacial and englacial features makes the surface and subsurface processes extremely important over the region. Hence, a study on the surface and subsurface temperature regimes of the region gives insights into the responses of these features to the temperature variations.

https://doi.org/10.5194/egusphere-2024-1666
Preprint. Discussion started: 11 June 2024

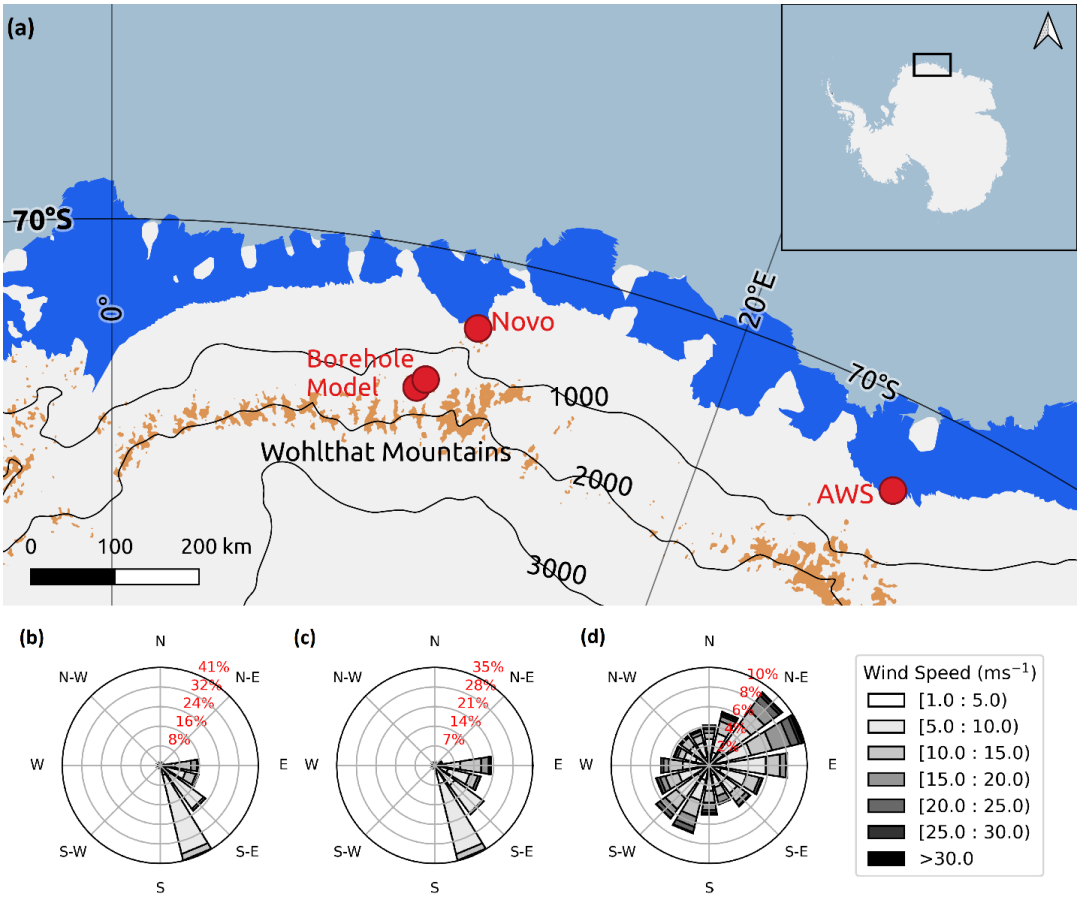

Figure 1: (a) Study region Coastal Dronning Maud Land with grounded ice (white) and ice shelves (blue) towards the coast. The scattered brown patches denote exposed rock outcrops. The locations of the borehole, Novolazarevskaya (Novo) station and AWS from Roi Baudouin Ice Shelf, and the nearest grid point in the RACMO2.3p2 model and ERA 5 to the borehole are marked as red dots. The region is near to a high mountain range called the Wohlthat Mountains and the surface slopes from the interior towards the coast (Lowther et al., 2022). The map of the study region is made using Quantarctica (Matsuoka et al., 2021). The black contour lines give elevation in meters, derived from the BEDMAP2m dataset. (b-d) Wind roses for the period 2014-2018 at the surface, at 850 hPa and 500 hPa levels, respectively from ERA5 dataset nearest to the borehole location. Radial lines give the percentage of occurrence of wind in that particular direction. Colour code represents wind speed with magnitude (in ms^{-1}) in the insect figure.

A set of thermistor-string assembly was deployed in the ice core borehole of an ice core (71.5 °S, 10.25 °E) during the austral summer of 2013-14 (Figure 1a), situated at 1470 m a.s.l. on a relatively flat region of ice sheet compared to the rock outcrops nearby, and close to the grounding line (~100 km inland) with slow ice-flow speed (3-4 myr^{-1}). Further inland of the location is the east-west oriented Wohlthat Mountains (Hui et al., 2014) ~ 20 km from the borehole location. The average air temperature from ERA5 reanalysis for the study period (2014-2018) was -22 °C and mean near-surface wind speed (10 m above surface) was about 8 ms^{-1} predominated by south easterly winds

https://doi.org/10.5194/egusphere-2024-1666
Preprint. Discussion started: 11 June 2024

(Figure 1(b-d)). These winds are cold and katabatic in nature originating from the elevated interior of the continent (Parish and Bromwich, 2007; Bromwich, 1989; Van Lipzig et al., 2004). Winds at 850 hPa (~ 1 km above sea level) are predominantly south-easterlies while the winds at 500 hPa (~ 5 km above sea level), are highly variable, blowing from all directions, but preferring a north-easterly direction.

In addition to the above wind structure, there are occasional surface easterly winds associated with cyclonic intrusions from climatological low centred at 25 °E that bring moisture and precipitation to the region (Noone et al., 1999; Schlosser et al., 2010). Such episodic high precipitation events contribute to the majority of the precipitation in the region and tend to heat the surface air to several degrees (even a T2m warming of 30 °C within a few days) (Hirasawa et al., 2000; Massom et al., 2004; Schlosser et al., 2010; Noone et al., 1999; Sinclair, 1981). cDML experiences an average of eight such warming events per year (Schlosser et al., 2010). In addition to the warm maritime air intrusions, wind scouring and melting are observed over some regions of cDML (Lenaerts et al., 2017). Being a region influenced by different meteorological and synoptic drivers favouring frequent atmospheric warming events, cDML serves as a suitable location to study the impact of these events on ISST under all meteorological conditions.

2.2 Borehole temperature measurements

The thermistor set assembly consists of 36 thermistors connected to thermometry strings placed in different levels (six thermistors above the surface up to 1.2 m and 30 thermistors below up to 30 m) and a data logger (DT 2040 RST instruments, Canada) (Supplementary Figure 1s). The placement of thermistors follows a tiered spacing pattern. Between 1 meter above the surface and 1 meter below, the sensors are installed at 20 cm intervals. At depths from 1 to 2 meters, the spacing increases to 25 cm, while from 2 to 4 meters, it is 50 cm. Beyond that, from 4 to 30 meters below the surface, thermistors are consistently spaced at 1-meter intervals. The sensors have an accuracy of 0.01 °C and were calibrated before deployment. The data logger was fixed next to the borehole in a 1-m pit and firmly secured to a bamboo stick. The thermistors were placed one day after drilling completion and started functioning from 5th January 2014 onwards, regularly taking measurements in 6-hour intervals. The data was retrieved from the logger twice, in December 2017, and December 2018.

2.3 Reanalysis and model data

Since continuous in-situ meteorological observations were unavailable at the borehole site for 2014-2018, we used the 5th generation ECMWF reanalysis (ERA5) data (Hersbach et al., 2020) to understand the mechanism of warming. The data gives hourly records of atmospheric parameters at the surface level with a grid resolution of 0.25°x 0.25°. The data obtained for the study are, (1) Components of Surface energy balance - Net shortwave and longwave radiation, total downward longwave radiation, sensible heat flux, and latent heat flux, (2) Meteorological conditions- wind speed and wind direction at the surface (10 m) and upper levels (850 hPa, 500 hPa), vertical velocity, cloud fraction, cloud base height, air temperature (2 m) and precipitation, (3) Synoptic conditions – Mean Sea level pressure.

The availability, consistency and high spatial resolution make ERA 5 an excellent choice for studying regions with limited data coverage like Antarctica. It has been used in several studies to represent upper-level meteorological conditions and accurately represent near-surface wind conditions (Tetzner et al., 2019). However, previous studies

https://doi.org/10.5194/egusphere-2024-1666
Preprint. Discussion started: 11 June 2024

reported its biases in representing the near-surface air temperature (Garza-Giron and Tulaczyk, 2023; Nielsen et al., 2023), while successfully representing general variability and trends (Zhu et al., 2021). To understand the biases, we compared the daily 2 m air temperature (T2m) of ERA5 with 2m air temperature measurement from Novolazarevskaya station (Russia, 70°46` S, 11°52` E), ~ 100 km coastward from the borehole location for a year (Supplementary Figure 2s). ERA 5 underestimated the temperature by a mean of ~ 2 °C. The bias is distributed uniformly in all seasons. This might introduce some errors in the estimation of absolute values of T2m warming near the borehole location. Nevertheless, the daily fluctuations of ERA5 agreed well with in situ data in terms of timing, making it suitable for a temporal comparison with borehole temperature time series.

Similar to other reanalysis datasets, previous studies reported biases in ERA 5 SEB fluxes over Antarctica due to limitations in the model physics (King et al., 2015). Silber et al (2019) observed biases in net shortwave and incoming longwave fluxes by magnitudes ± 100 Wm^{-2} and ~50 Wm^{-2} respectively over West Antarctica in comparison with in situ measurements largely due to inaccurate representation of cloud phase in the model. To assess the accuracy of ERA5 SEB fluxes over cDML, we compared it with two datasets: daily AWS observations from Roi Baudouin Ice Shelf in Dronning Maud Land (70.95°S, 26.27°E) (Jakobs et al., 2020b, a) and monthly RACMO2.3p2 model output from a location near the borehole (71.4°S,10.5°E) (van Wessem et al., 2018). ERA 5 overestimated the monthly SEB fluxes (LWnet, SHF and LHF) compared to the SEB fluxes from the RACMO2.3p2 model, but showed good correlation with the model fluxes (Supplementary Figure 3s).

The daily SEB fluxes of ERA 5 were compared with an AWS for the summer and winter of 2015 (Supplementary Figures 4s & 5s). For both seasons, all the SEB fluxes from ERA5 were mostly overestimated with a large amplitude of fluctuations compared to the AWS data. The bias is reduced for the net heat flux. Although the absolute values of ERA 5 deviated from observation, the overall pattern is mostly in agreement with in situ data. Ghiz et al (2021) observed qualitative consistency between in situ net energy flux and ERA5 over West Antarctica and therefore used ERA 5 SEB fluxes to assess the mechanism of melting events in their analysis. Because of the biases in the absolute values of SEB fluxes, we also limit the use of ERA 5 SEB fluxes for the qualitative understanding of the events.

2.4 Calculation of subsurface conductive heat flux and determination of surface energy balance

Surface energy balance (SEB) is the sum of all the incoming and outgoing energy fluxes. The net heat flux (Q),

$$Q = SWnet + LWnet + SHF + LHF + G \quad (1)$$

Where ‘SWnet’ is the net shortwave radiation (sum of incoming and outgoing shortwave radiation), ‘LWnet’ is the net longwave radiation (sum of incoming and outgoing longwave radiation), and SHF is sensible heat flux. LHF and G are Latent heat flux and subsurface conductive heat flux respectively. All the fluxes are positive when directed toward the surface. LHF is negative for sublimation and positive for condensation. G is positive when directed towards the surface and negative when directed into the snowpack. All the parameters except G are obtained from the ERA5

https://doi.org/10.5194/egusphere-2024-1666
Preprint. Discussion started: 11 June 2024

dataset from a grid point near the borehole. The G is calculated from the surface and subsurface temperature measurements, using Fourier's law of heat conduction;

$$G = -Ke\frac{dT}{dz} \quad (2)$$

Where T is the temperature and z is the depth (negative downwards). The heat flux towards the ice pack is negative, whereas towards the surface is positive. The heat flux between each layer is calculated using the temperature measurements of 20 thermistors from the surface to a 10 m depth and the respective spacing between them: spacing between thermistors (dz) varies by 20 cm (between the surface and 1 m), 25 cm (between 1 m and 2 m), 50 cm (between 2 m and 4 m), and 1 m (between 4 m and 10 m). The final depth for calculation of G is considered as 10 m, since, there is no penetration of heat after this level for the period we studied. Finally, all the individual fluxes are added to get the net conductive heat flux (G). Ke (in W m^{-1} K^{-1}) is the effective thermal conductivity and is estimated as a function of density (ρ in kgm^{-3}) using the equation (Östin and Andersson, 1991).

$$Ke = -0.00871 + (0.439 * 10^{-3})\rho + (1.05 * 10^{-6})\rho^2 \quad (3)$$

ρ at each level is directly obtained by measuring the top 10 m ice core sections. Short-wave penetration into the snowpack was neglected for fine-grained, dry Antarctic snow (Brandt and Warren, 1993). For the present study, the estimated G serves two purposes: acting as a closure term for the SEB from ERA5 and understanding the role of subsurface conduction in stabilizing the ISST during warming. Supplementary Figure 3s shows the comparison of calculated G in the present study with the monthly subsurface heat flux of the RACMO2.3p2 model. The estimated G agrees with the model output. Furthermore, the net heat flux of ERA5 and the model deviated at some points when G was not included but showed a good correlation when G was included in the calculation of SEB.

The sublimation rate (in m.w.e) of the surface is calculated from latent heat flux (LHF) and latent heat of sublimation, Ls (2.83 x 10^6 Jkg^{-1}) and ρw is the density of water.

$$Sublimation\ rate = \frac{\mathrm{LHF}}{Ls * \rho w} \quad (4)$$

2.5 Retrieval of ice sheet surface temperature

Supplementary Figure 6s represents the daily average temperature measured at the surface level thermistor from 2014-2018. The maximum and minimum temperature recorded over a year decresed over the period 2014-2018, from -6.2°C to -14.8°C and -38.1°C to -34.5°C while yearly average remained same (~ -25°C). This suggests that, over the years, the amplitude of day-to-day fluctuations in the surface-level thermistor decreased. This dampening in temperature was the result of the burial of thermistors each year by the annual snow accumulation. In other words, the surface level thermistor during the deployment no longer records the surface temperature by 2018, but rather gets buried by each year's snow accumulation. The buried thermistors record smaller fluctuations than the surface thermistors, and the

https://doi.org/10.5194/egusphere-2024-1666
Preprint. Discussion started: 11 June 2024

exposed ones record larger fluctuations. This is evident from the profile of temperature at different levels for summer and winter shown in Fig. 6s (c) and (d)).

To quantify the burial, the average annual accumulation of the period is determined. This gave the approximate time to shift to the next upper-level thermistor measurement (as surface temperature) until this new one gets buried by the respective year's snow. Since there was no in situ measurement of annual accumulation, we examined the surface mass balance of the RACMO2.3p2 model run at 27 km resolution near the borehole location (van Wessem et al., 2018), which considered all the influxes and out fluxes (total precipitation, sublimation, and snow drift) of surface mass balance. Table 1 gives the annual surface mass balance from RACMO2.3p2 for 2014-2018.

Table 1: Surface mass balance data from the RACMO2.3p2 model for the nearest grid point to the borehole location, covering the period from 2014 to 2018. Surface mass balance is the sum of all the accumulation and ablation processes.

Year	Surface mass balance from RACMO2.3p2 (cm.w.eq)
2014	11.8
2015	11.1
2016	11.0
2017	9.5
2018	9.8

The average annual surface mass balance for the region was ~10 cm.w.eq /year for 2014-2018, meaning the thermistors would have buried by ~ 10 cm each year. We used this value as a reference for the burial of surface thermistors which were later modified manually by maintaining uniformity in temperature fluctuations (Noone et al., 1999). Accordingly, we took surface temperature values from the sensor on the surface when installed for January 2014-September 2015, a height of 20 cm for October 2015-December 2017, and finally, 40 cm for 2018. Supplementary Figure 6s (b) shows the final temperature time series after considering burial. The depths selected may not be accurate due to biases in the precipitation and sublimation data and the large spacing between thermistors (20 cm). However, the errors in depths of +/- 20 cm can be permissible since these levels correlate well with the surface (r-value between 20 cm above and surface = 0.986 and between 20 cm below and surface =0.987. Both the values have $p < 0.001$). The time series of temperature at the surface level, 20 cm above the surface and 20 cm below the surface for 2014 (Supplementary Figure 7s) shows that all the fluctuations were synchronous at the three levels with different amplitude of fluctuation. There was a horizontal movement of sensors parallel to the region's ice flow (3-4 m yr^{-1}). Since it does not affect our study, its horizontal movement with time was ignored.

https://doi.org/10.5194/egusphere-2024-1666
Preprint. Discussion started: 11 June 2024

2.6 Selection of warming events

The daily average temperature profile of the ice sheet surface had some day-to-day variability superimposed on seasonal variability (Supplementary Figure 6s (b)). These sudden rises in ISST for a brief period are considered as ISSW events. The onset of an event is identified when the temperature begins to rise. The end of the event is marked when the temperature either decreases or stabilizes. This criterion ensures consistency, as during the summer months, ISSW does not show a distinct decrease but stabilizes before rising again due to seasonal warming. Thus, defining the end of an event by the day before a decrease or stabilization of temperature provides uniformity in the duration of ISSW of all seasons. Figure 2 shows two ISSW events with the duration of events shaded in blue. The temperature from 26 Sep - 6 Oct 2015 stabilized after 6 October, marking the event's end. A similar feature was observed during 27 Sep -03 Oct 2017. The magnitude of warming of each event was the difference between the temperatures of the end and start dates and the duration was the number of days between the start and end dates. There were 140 events during the study period with a warming of 0.2 °C to 11 °C. Supplementary Figure 8s shows the histogram of warming extent for all the events. Among the events, ~50 % of the warming was small in magnitude (< 2 °C). The warming in this range can have more biases due to errors in the selection of surface level compared to higher warming. Hence, we incorporated the top 50 % of warming events, with warming greater than 2 °C as a threshold for warming events. These events had a duration greater than or equal to 3 days. The T2m warming during the events above this threshold was large ranging from 5-20 °C, and rapid fluctuations in this range are sufficient enough to change the firn properties of ice sheets (McDowell et al., 2020). Hence, by applying this selection criterion, we sorted 70 ISSW events from cDML for the period 2014-2018. These events were examined for their general meteorological conditions, mechanism of warming and synoptic conditions favouring it.

https://doi.org/10.5194/egusphere-2024-1666
Preprint. Discussion started: 11 June 2024

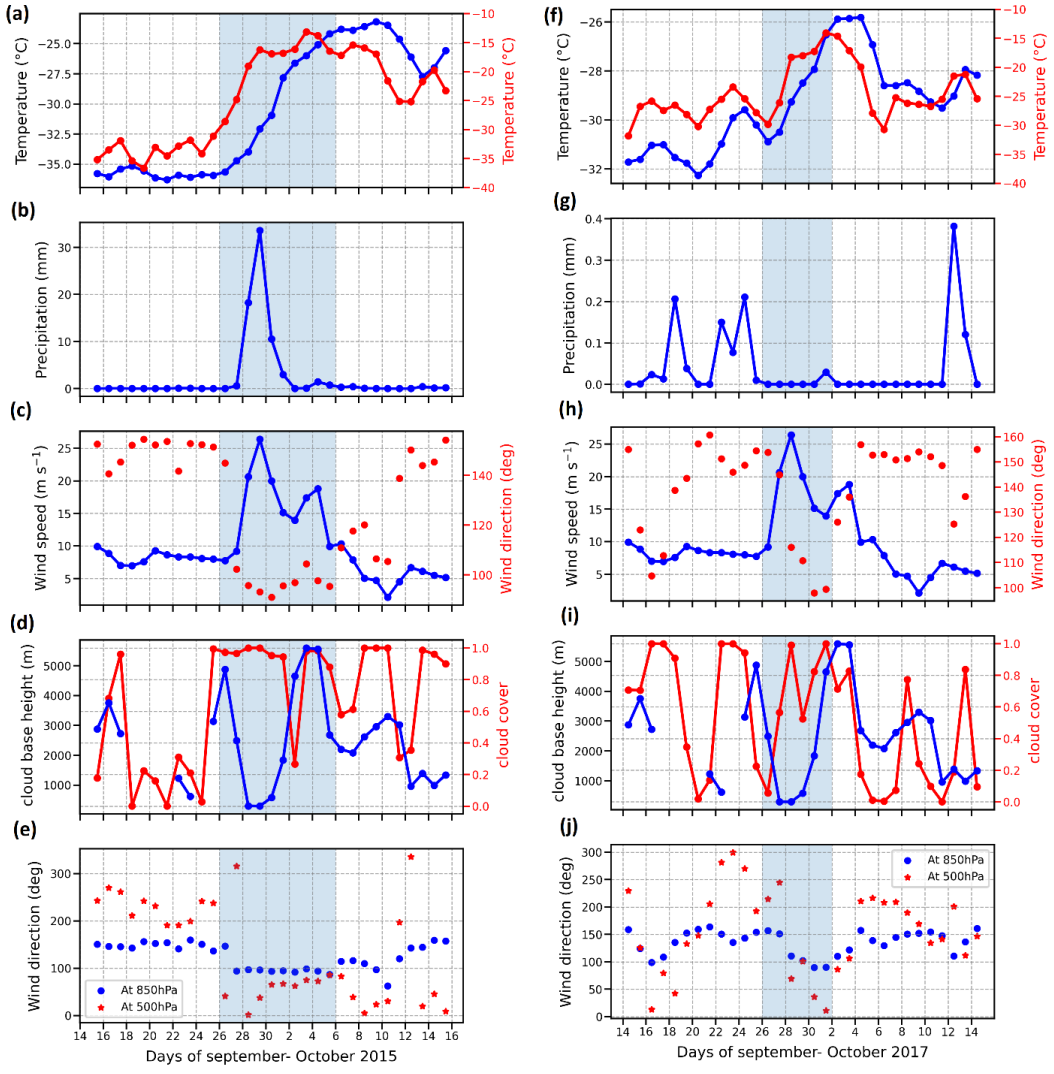

Figure 2: (a -e) Meteorological conditions of an ISSW event with surface easterly winds. The shaded region marks the beginning and end of each event. Onset is taken when the borehole temperature (ISST) starts to increase and ends when the temperature stabilizes or decreases. (a) The ISST (blue) and T2m (red), (b) Precipitation, (c) Wind speed as blue line and wind direction as red dots at the surface level (10m), (d) Cloud cover (red) and cloud base height (blue) and (e) wind directions at 850 (blue dot) and 500hpa (red star) levels. (f-j) Same as (a-e) but for an ISSW event with surface southeasterly winds. All the parameters except ISST were obtained from ERA5 near the borehole location.

3. Results

3.1 Ice sheet surface warming (ISSW) events

The daily average temperature at the borehole surface recorded during 2014–18 CE is presented in Figure 3a**.** The dashed vertical lines represent the ISSW events identified by the criteria mentioned above. There were 70 significant warming events recorded for the period, with a temperature increase of 2 °C to 11.75 °C and lasting between 3 to 10

https://doi.org/10.5194/egusphere-2024-1666
Preprint. Discussion started: 11 June 2024

days. The yellow bar in Figure 3b shows the number of events annually for the period. We find that 2016 had the most number of warming events (18) followed by 2017 (15) and 2018 (14), while the year 2014 recorded the least number of events (8). Among these events, the majority (46 ISSW events) were reported during spring and winter (23 each), followed by autumn (14) and least during summer (8). January was the only month devoid of any ISSW events.

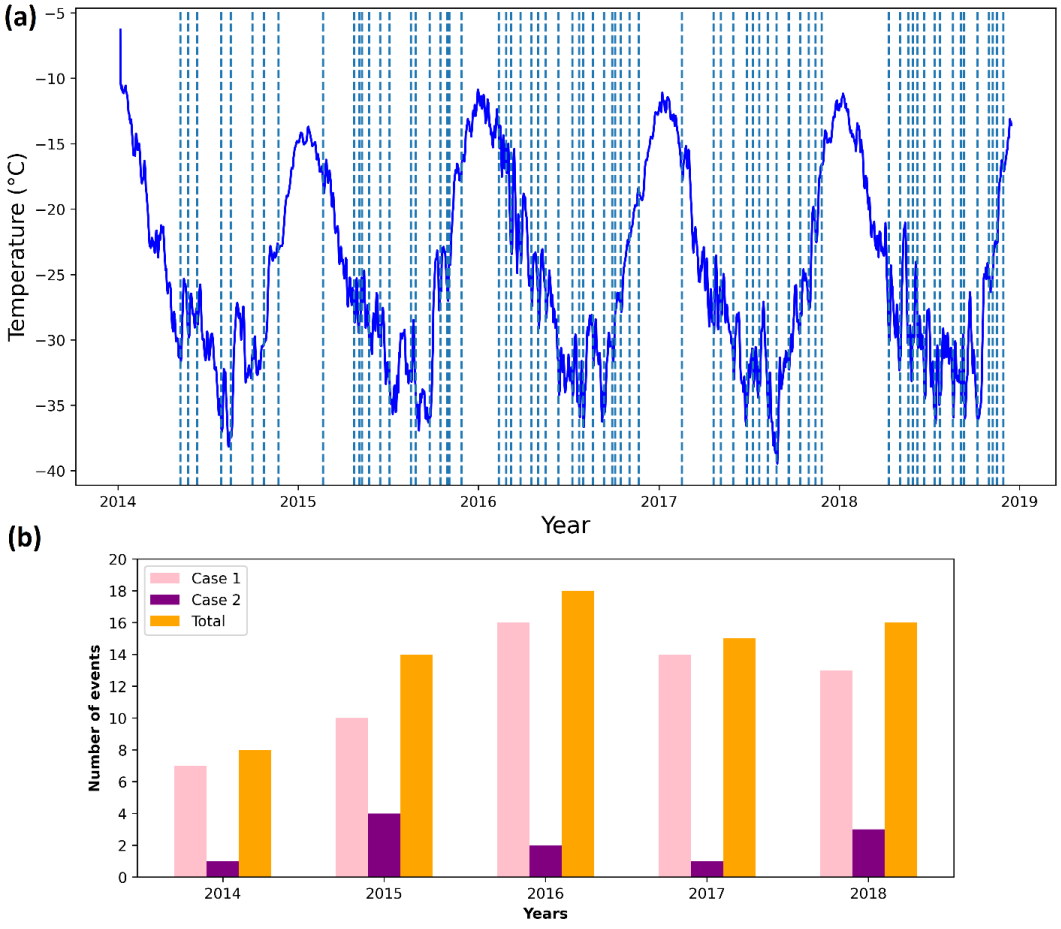

Figure 3: (a) Time series of daily average ice sheet surface temperature from borehole thermistors for the time period 2014-2018. Dashed lines represent the ISSW events. (b) The annual number of warming events during the study period. The color bars are; pink- case 1 (ISSW events with surface easterly winds), violet – case 2 events (ISSW events with surface south easterly winds) and orange – the sum of case 1 and case 2.

The general meteorological conditions of the events revealed two distinct features. Out of 70 warming events, 60 were associated with surface easterly winds and snow precipitation (>1 mm), while the rest 10 events had surface southeasterly winds without any precipitation. Hence we categorized the events based on their meteorological features, that is events associated with surface easterly winds and surface southeasterly winds. In the later sections, we examine one case study from each category that occurred during the same time of year with high ISSW, to analyze the warming features (extent and timing) of ISST, T2m and subsurface temperatures. We also examine their mechanism of warming

https://doi.org/10.5194/egusphere-2024-1666
Preprint. Discussion started: 11 June 2024

and synoptic drivers and finally demonstrate the frequency and seasonality of similar ISSW events over the study period.

3.2 ISSW associated with surface easterly winds

3.2.1 Case study

The ISSW event from 26 September to 5 October 2015 resulted in a warming of 11.7 °C, the highest surface warming recorded over the borehole surface temperature of cDML for the study period (Figure 2a). The near-surface wind speed was high during the period, preferring an easterly direction (Figure 2c). The region experienced snow precipitation for four days from 28 September to 1 October. 2m air temperature (T2m) started warming two days before the ISSW, on 24 September and persisted till 3 October causing a warming of ~20 °C. Figure 4(a-f) shows the surface energy balance components during the event. The SW_{net} was minimal during the event hence contributing less to warming. LWnet loss from the surface decreased from 24 September with a small peak on 25 September and continuously raised the LWnet value to near zero for 28-30 September. The LWnet was high during the event until 1 October 2015, later decreased. The reduced LWnet loss enhanced net radiation during the event and significantly contributed to surface warming.

https://doi.org/10.5194/egusphere-2024-1666
Preprint. Discussion started: 11 June 2024

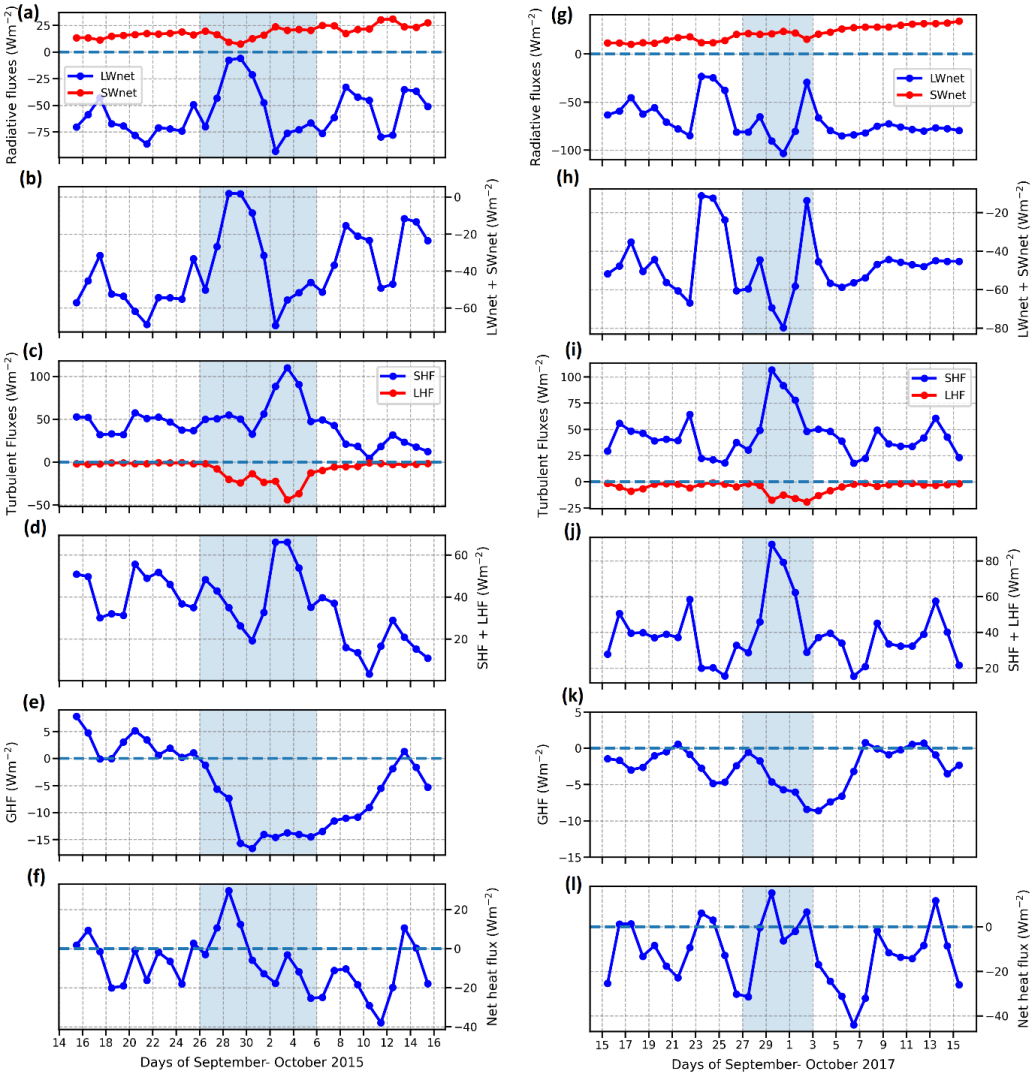

Figure 4: (a -e) The daily mean surface energy balance of the ISSW event with surface easterly winds with shaded region representing the duration of the event. (a) Radiative fluxes – net longwave radiation (LWnet) in blue and net shortwave radiation (SWnet) in red, (b) Net radiation as sum of radiative fluxes, (c) Turbulent fluxes, sensible heat flux (SHF) in blue and latent heat flux (LHF) in red, (d) Net turbulent flux as sum of SHF and LHF, (e) Ground heat flux (GHF), and (f) Net heat flux as sum of all SEB components. (g-l) Same as (a-f) but for the ISSW event with surface south easterly winds. All the parameters except GHF were obtained from ERA5 near the borehole location. GHF was estimated from borehole thermistor measurements using Eq. (2).

LWnet value over the surface increases when downward longwave radiation (LWD) towards the surface increases, and it is dependent on several factors such as the nature of cloud and air temperature (Sato and Simmonds, 2021). Figure 2d represents total cloud cover (both low and high clouds) over the region. There was high cloud cover from 25 September to 1 October emitting LWD for the period. High-level clouds (>2 km) appeared for 24 – 28

https://doi.org/10.5194/egusphere-2024-1666
Preprint. Discussion started: 11 June 2024

September associated with a weak warm air advection and resulted in initial warming of air temperature on 24 September. Later, from 28 September to 2 October, the region experienced low-level clouds that emitted strong LWD towards the surface.

The role of turbulent heat flux in ISSW is observed only towards the end of the events. The turbulent heat flux was minimal during the first half of the warming event from 24-30 September (when net radiation was high), but increased from 1 October to the end of the ISSW event (5 October). The largest contributor to turbulent heat flux was SHF which peaked at a high value of 110 Wm^{-2} on 3 October, when air temperature recorded its highest value of -24 °**C**. Strong SHF from the warm air above heated the Ice sheet surface for two more days (3-5 October) after the end of T2m warming.

The ground conductive heat flux was small and positive before the ISSW event, meaning that the heat flowed from the warm subsurface to the cold surface layer (Figure 4e). G became negative from 26 September onwards (when the ice sheet started warming) and by 29-30 September, it reached -15 Wm^{-2} and removed excess energy from the surface to the subsurface. Later, it almost remained stable until 6 October and reduced afterwards. The net heat flux remained positive for 26-30 September, when the surface witnessed radiation excess subsided afterwards (Figure 4f).

On 23 September, a low-pressure system was present over the Weddell Sea near the Antarctic Peninsula (Figure 5a). On the first day of T2m warming (24 September), the low-pressure system moved eastward towards cDML and induced a weak warm air advection towards the region (Supplementary Figure 9s (a)). Later, it moved eastwards and remained stationary off the coast of cDML due to the blocking effect of an anticyclone formed eastward of the cDML from 27-30 September, when the Ice sheet surface started warming (Figure 5b). The region experienced direct warm air advection from the low-pressure system from 27-30 September, which led to low-level cloud formation and cloud-induced LWD. For the next day (1 October), the low-high system shifted to the east of its former location and remained stationary for the next four days (till 5 October) due to blocking (Figure 5c). During this time, the location aligned with the system's western flank, facilitating high wind speed at the surface and inducing strong turbulent heat flux for the latter half (1-5 October) of ISSW (Figure 5d).

https://doi.org/10.5194/egusphere-2024-1666
Preprint. Discussion started: 11 June 2024

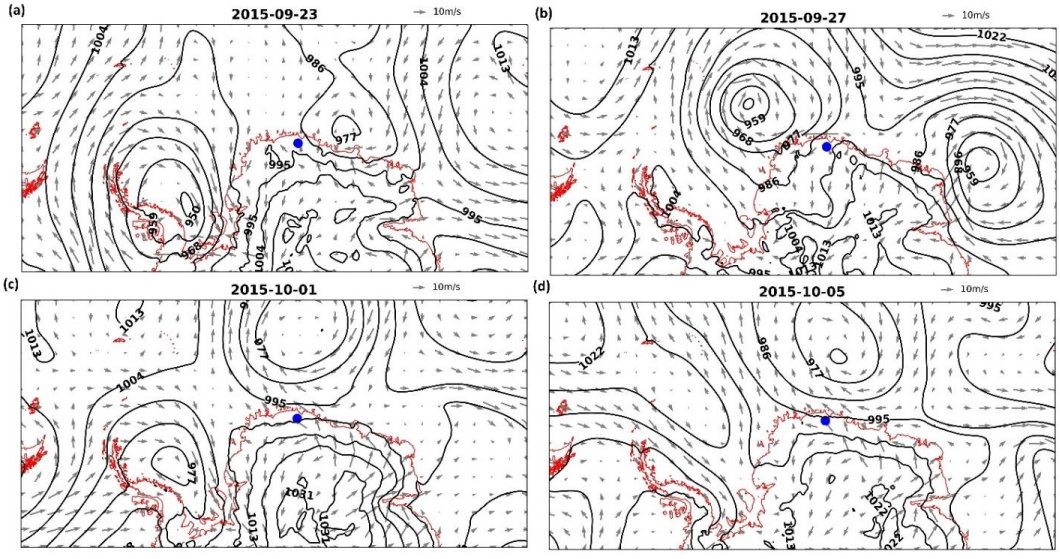

Figure 5: (a -d) The daily mean sea level pressure (MSLP) and surface level wind vectors for some days during the ISSW event of 26 September – 06 October 2015. The borehole location is marked as blue dot. All the parameters were obtained from ERA5.

The ISSW in this case was lagged by two days compared to T2m warming. The T2m warming began when a low pressure appeared over the Weddell Sea that resulted in a weak warm air advection. ISSW began only after two days when the low pressure moved further east advecting direct warm, moist air towards the surface. Low-level clouds associated with these warm air advection episodes heated the ice sheet surface via strong LWD emission. It remained stationary due to a blocking anticyclone and continued warming the atmosphere and ice sheet surface. Subsequently, as warm air advection and the accompanying cloud disappeared from the area, LWD decreased, resulting in the cessation of T2m warming. However, the ISSW sustained for two more days due to strong SHF from the warmer air above.

3.2.2 Subsurface conditions during the event

The profile of G followed the subsurface temperature profile (Figure 4e & 6a). The lowest layers were warm before the commencement of ISSW and the immediate layer close to the surface (20cm) started warming (on 26 September) together with the surface without any lag. The subsurface depths of 40 and 60 cm started warming one day later, on 27 September and 80 cm after two two-day lag with the surface (on 28 September).

https://doi.org/10.5194/egusphere-2024-1666
Preprint. Discussion started: 11 June 2024

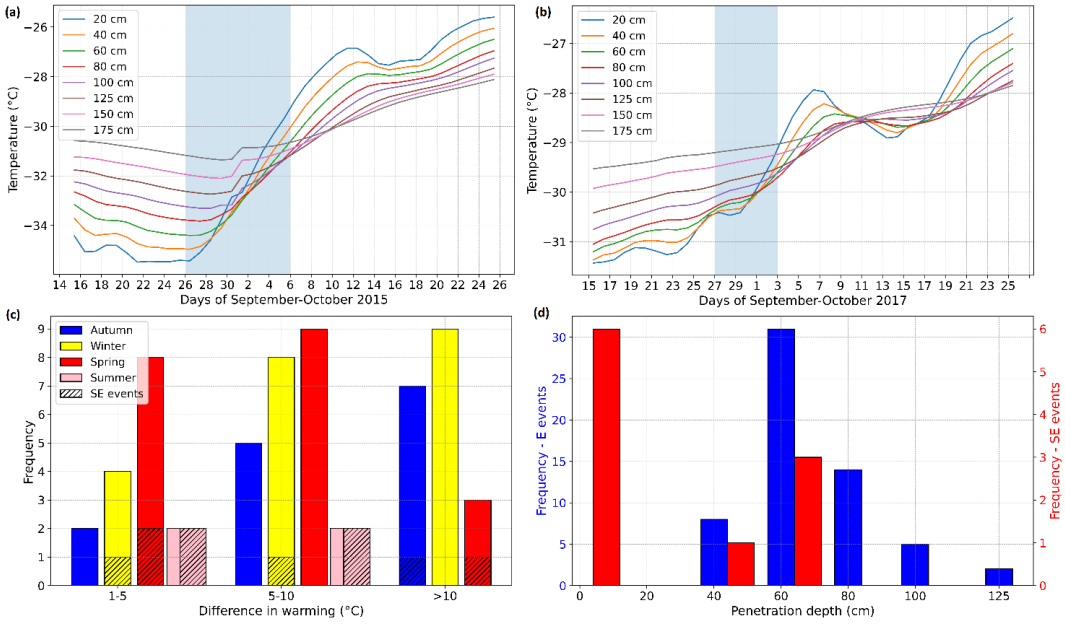

Figure 6: (a) The daily mean subsurface temperature time series during the ISSW event of 26 September – 06 October 2015 with shaded region marking the duration of ISSW. (b) Same as (a) but for ISSW event of 27 September – 03 October 2017. (c) Histogram of difference in warming (T2m-ISST) for surface easterly (solid bars) and southeasterly (dashed bars) winds season wise. X axis shows difference in regular intervals and Y axis shows the number of events. (d) Histogram of maximum penetration depth for Easterly wind events (blue) and south easterly wind events (red). None of the events showed a maximum penetration depth of 20 cm. All the parameters were obtained from borehole thermistor measurements.

We define the maximum depth heat penetration for an event as the deepest layer that shows distinct start and end days of warming similar to the warming pattern of ISST. The maximum depth of heat penetration for this warming event was 80 cm, below this layer, the signal dampened daily fluctuations and followed continuous seasonal warming. The temperature gradient between the surface layer and the subsurface layers was maximum for 29-30 September since the subsurface layers lagged, resulting in increased downward G. Table 2 shows the start date, end date and magnitude of warming of air and ice sheet surface layers. The magnitude of warming decreased from the surface to deeper layers. The warming of the depth of maximum penetration (80 cm) was almost reduced to half as that of surface level and the warming lagged by two days. It is to be noted that the subsurface layers (20-80 cm) took a longer time to reach the highest temperature, especially 20 cm (lag of 6 days) and other layers with a lag of one day from their respective upper layer. After the end of the event, the temperature profile followed the seasonal cycle.

https://doi.org/10.5194/egusphere-2024-1666
Preprint. Discussion started: 11 June 2024

Table 2: The start date, end date and the magnitude of warming of T2m, ISST and subsurface layers for the case study from 26 September – 06 October 2015. T2m was obtained from ERA5 for a nearest grid point to borehole location. The ISST and subsurface tempertaures were measured by borehole thermistors.

Level	Start date	End date	Warming (°C)
T2m	24-09-2015	03-10-2015	~20
ISST	26-09-2015	05-10-2015	~11
20 cm	26-09-2015	11-10-2015	8
40 cm	27-09-2015	12-10-2015	7.5
60 cm	27-09-2015	13-10-2015	6.5
80 cm	28-09-2015	14-10-2015	5.5
100 cm	30-09-2015	Continuous increase	

3.2.3 Similar ISSW events of cDML

Out of the 70 ISSW events, 60 events were in the category of warming associated with strong surface easterly winds (greater than average). They resulted in near-surface atmospheric warming in the range of 4.4 – 24.6 °C and ISSW in the range of 2 -11.7 °C, including the top 19 ISSW events (warming from 5-11.7 °C). For the period 2014-2018, the annual frequency of these events varied from year to year with an average occurrence of 12 events per year (Figure 3b). They occurred frequently during winter (21), spring (20), autumn (14) and summer (5).

Figure 7a represents composite of Mean Sea Level Pressure (MSLP) anomaly and MSLP contours during the events. During the events, the region covering the location was within a low-pressure system. They resulted in warm, moist air advection and induced warming over the region by cloud cover and warm air above. Similar to the case study, when surrounded by high-pressure systems to the east, they resulted in the blocking of the eastward progression of low pressure for some days and favoured prolonged warm air advection and ISSW over the region.

https://doi.org/10.5194/egusphere-2024-1666
Preprint. Discussion started: 11 June 2024

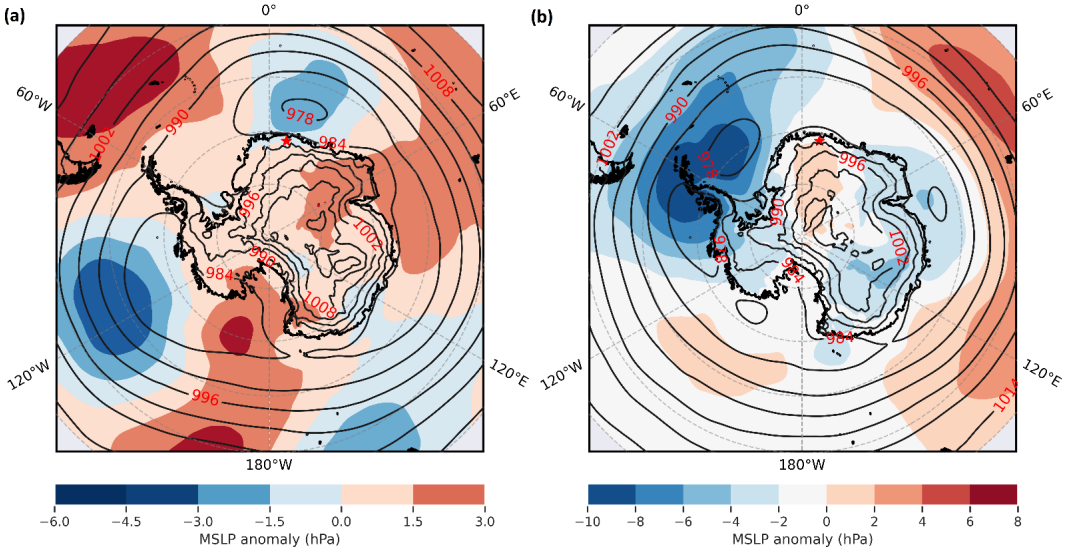

Figure 7: (a) Composite of Mean Sea Level Pressure (MSLP) anomaly (filled contours) and MSLP contours for ISSW events with surface easterly winds. (b) Same as (a) but for surface southeasterly wind events. Climatology is calculated for 1979-2018 from the ERA5 dataset. The borehole location is marked as red star.

For these events, the correlation between net heat flux and net radiation was higher (r = 0.54, p<0.001) than that between net flux and turbulent flux (r = 0.27, p<0.001**),** implying that the net radiation had more influence on net heat flux. The contribution of net shortwave radiation in net radiation for all these events (summer and winter combined) was much less (r = 0.37, p<0.001) compared to net longwave radiation (r = 0.67, p<0.001). This suggests that increased LWD from the atmosphere dominantly warmed the ice sheet surface. Although the contribution of turbulent heat flux in net heat flux is small, its positive contribution cannot be ignored, especially in the final days to maintain the ISSW beyond T2m warming, as observed in the case study.

The time lag between air warming and ISSW was two days for the case study, the former leading the latter. The correlation between air temperature and ISST during these events was maximum (r=0.85,p<0.001) when a two-day lag was applied between air and surface compared to no lag (r = 0.78,p<0.001), suggesting that air leads the surface for two days for all these events. Although the absolute values of ERA5 2m temperature and ISSW have individual biases, we compared the temperature difference between them to understand the difference in the extent of their warming. The difference between T2m warming and ISSW was in a range from 1.3 to 16.2 °C. Figure 6c shows the histogram of the difference in T2m warming and ISSW. Mostly, events with the largest differences occurred during autumn and lowest during summer (2 °C) and spring (1.3 °C).

We examined the maximum depth of heat penetration for all the events following the same criteria as the case study. Figure 6d shows the histogram of the maximum depth of heat penetration of events. The depths varied from 40 – 125 cm, with a large number of events in the range of 60-80 cm. The results show that the effect of these events can reach the top 40-125 cm of firn.

https://doi.org/10.5194/egusphere-2024-1666
Preprint. Discussion started: 11 June 2024

3.3 ISSW event associated with surface south easterly winds

3.3.1 Case study

The ISSW event from 27 September to 3 October 2017 recorded the highest ISSW (~5 °C) recorded in this category of events (Figure 2f). Strong surface-level south easterlies from the interior of the continent prevailed during the event (Figure 2h). The T2m started warming on the same day as ISSW (27 September) and ended one day before the ice sheet (on 2 October) recording an overall warming of 15 °C. After 2 October, T2m cooled but ISST remained stable until 5 October before cooling and following the pattern of T2m.

Figure 3 (g-l) represents the SEB components during the ISSW event. Similar to the previous event, SWnet during the period was less and insignificant in contributing to surface warming. LWnet losses were high at the beginning of warming (27-30 September), indicating a lower contribution to surface warming. Towards the end of the event (after 1 October), LWnet loss decreased for two days resulting in a small rise in ISST. Thus, unlike the previous event, the ISSW was not caused by enhanced net radiation. The notable difference between this event and the previous case study was strong turbulent heat flux, especially increased SHF from 27 September to 1 October, which resulted in ISSW.

Elevated SHF over Antarctica can result from increased air temperatures due to warm air advection from low latitudes. However, the surface-level wind pattern in this case showed a southeasterly wind of continental origin (Figure 2h). Similarly, at 850 and 500hPa levels, the wind direction was southeasterly and southwesterly respectively at the beginning of ISSW (from 27-29 September) (Figure 2j). The wind direction changed to easterly and northeasterly after 29 September, resulting in a small rise in LWnet from warm air advection and intermittent cloud cover (Figure 2i).

The ground conductive heat flux was negative (towards the subsurface) but small one day before (26 September) the beginning of ISSW (Figure 4k). Later, when the ISSW started, the G increased in the negative direction, towards the subsurface and reached its highest value by the end of the event (2-3 October). The maximum value of G was small (~ -8 Wm^{-2}) compared to the previous ISSW event. The profile of net heat flux closely followed the turbulent heat flux (Figure 4l).

To understand the mechanism of warming associated with surface southeasterly winds, we examined the synoptic conditions of the event. Figure 8 (a-c) shows the mean sea level pressure and near-surface wind vectors for the event.

https://doi.org/10.5194/egusphere-2024-1666
Preprint. Discussion started: 11 June 2024

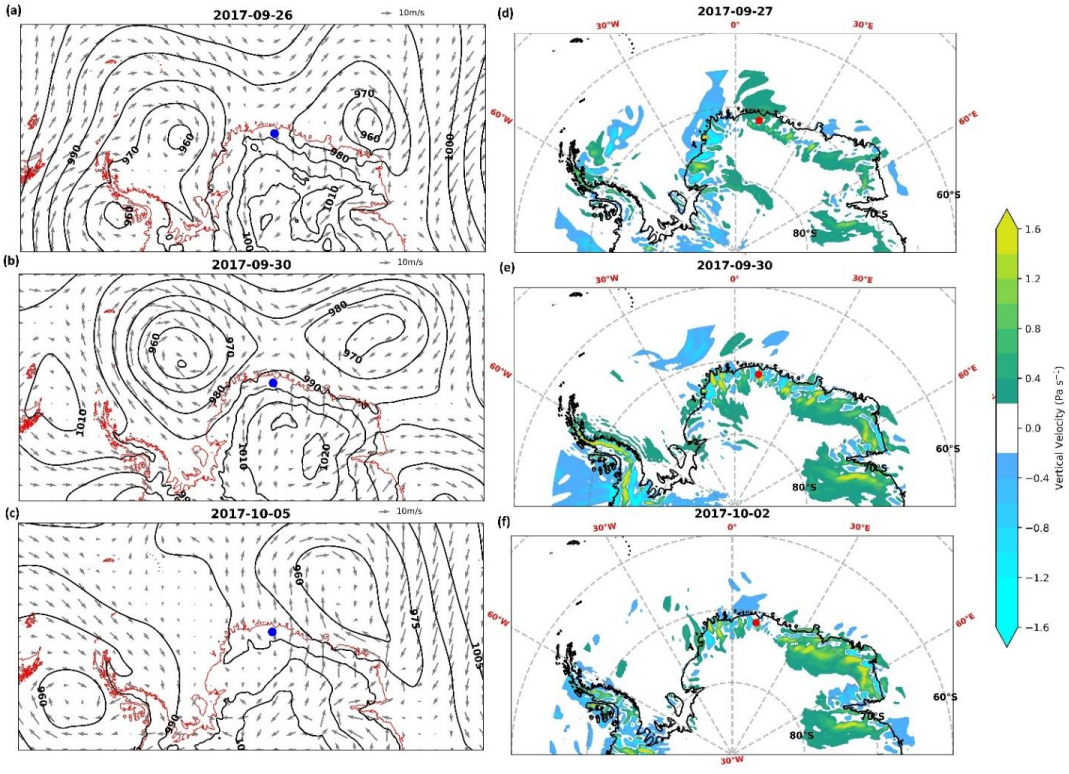

Figure 8: (a -c) The daily mean sea level pressure (MSLP) and surface level wind vectors for some days during the ISSW event of 27 September – 03 October 2017. The borehole location is marked as blue dot. (d-f) The 700hPa level vertical velocity for 12 UTC of some days during the event. Positive values indicate sinking. The borehole location is marked as red dot. All the parameters were obtained from ERA5.

At 12 UTC of 26 September, a low-pressure system was present over the Weddell Sea with a high-pressure system over cDML and its coast (Figure 8a). The movement of the low-pressure system was blocked by the high-pressure system for the next three days until 30 September (Figure 8b). The system moved off the coast of cDML with intermittent warm air intrusion (thereby leading to cloud formation) further east of the region by 5 October. Similarly at 500hPa level troughs were formed over the Weddell Sea by 26 September, directing warm, moist air towards the western DML (Supplementary Figure 9s (b)). The ridges present over the cDML and its coast facilitated consistent warm air intrusion to the inland of the continent by blocking the troughs until 30 September. Figure 8d shows the 700hPa level vertical velocity profile when ISSW started over the location (27 September). The coastal region beyond 0 °E had strong sinking air that persisted till 30 September (Figure 8e), afterwards as the low system progressed to the east the sinking reduced over the location (Figure 8f). This suggests that the warm airmass that advected towards the interior of the continent, experienced a blocking by the high topography of the inland region, recurved its path and descended towards the coastal regions. This airmass warmed adiabatically upon its descent from inland and resulted in T2m warming over cDML from 27-29 September. After 30 September, the low-pressure system progressed off the

https://doi.org/10.5194/egusphere-2024-1666
Preprint. Discussion started: 11 June 2024

cDML coast towards the east, along its track intermittently inducing warm air advection and cloud formation over the region. This resulted in the low LWnet loss for two days until 3 October.

Initially (27-30 September), the mechanism of ISSW associated with surface southeasterly winds was strong turbulent heat flux from the warm air above the surface, but later warmed for a few more days (1-3 October) by LWD from intermittent cloud cover. The air and the surface warmed together without any lag/lead. From 27-29 September, a low-pressure system prevailed over the Weddell Sea blocked by a high-pressure over the cDML, which directed warm air to the inland. Blocked by the elevated terrain of the inland, the air mass descended to coastal regions and warmed adiabatically. Later (1-3 October), as the blocking high pressure weakened, the low pressure progressed east along the track intermittently advecting warm air and facilitating cloud cover. Similar warming from recurving winds from the interior was first reported by Turner et al. (2022) in the Indian Ocean sector of East Antarctica associated with an atmospheric river event.

3.3.2 Subsurface conditions during the event

Figure 6b shows the subsurface temperature profile of the event. Before the commencement of the event, the subsurface was warmer than the surface. This profile is reversed when the surface warmed, followed by a 20 cm layer one day after (28 September). The layers 40 and 60 cm started warming with a two-day lag from the surface, by 29 September. The maximum depth of heat penetration for this event was 60 cm, below which the layers followed the seasonal trend with no exact start or end dates. Table 3 represents the start date, end date and magnitude of warming for each layer for this ISSW event. Subsurface layers (20-60 cm) warmed uniformly with a warming of almost half (~2.5 °C) of the surface layer (~ 5 °C).

Table 3: Same as Table 2, but for the event from 27 September to 03 October 2017.

Level	Start date	End date	Warming (°C)
T2m	27-09-2017	02-10-2017	15
ISST	27-09-2017	02-10-2017	5
20 cm	28-09-2017	06-10-2017	2.5
40 cm	29-09-2017	06-10-2017	2.5
60 cm	29-09-2017	06-10-2017	2.5
80 cm	29-09-2017	06-10-2017	2.5

https://doi.org/10.5194/egusphere-2024-1666
Preprint. Discussion started: 11 June 2024

3.3.3 Similar ISSW events of cDML

Warming events associated with strong surface southeasterly winds occurred only 10 times during the study period. They resulted in a warming of 2-5 °C over the ice sheet surface with an air warming of 4.9 -15.8 °C without any lag between them. The events mostly occurred in summer (4) and spring (3) followed by winter (2) and autumn (1).

On analyzing the energy balance in this case, we observed that net heat flux was greatly influenced by turbulent heat flux ($r = 0.37$, $p<0.001$) rather than net radiation ($r = 0.13$, $p =0.01$), pointing out that turbulent flux has caused surface warming. The correlation between air temperature and ISST was very high ($r = 0.88$, $p<0.001$) during these events compared to the easterly wind events. This implies that the ISSW were associated with the warming of the air above.

Figure 7b shows the composite of MSLP anomaly and MSLP contours during these events. The location had a weak high pressure flanked by low pressures on both sides. Unlike the previous case of easterly winds, the low pressure system is shifted to further west towards Weddell Sea. This configuration of low and high pressure induced an anticyclonic circulation over the region, driving more southerly winds and adiabatic warming similar to the case study.

The difference between air warming and ISSW was in the range of 1-11 °C with the highest difference occurring during autumn (11 °C) and spring (10 °C) and lowest in summer (1 °C) **(**Figure 6c). The subsurface warming during these events was restricted to four events only with a shallow heat penetration depth of 40-60 cm **(**Figure 6d). For the rest of the events, the subsurface followed a seasonal pattern without any marked start or end dates **(**supplimentary Figure 10s). This suggests that, unlike the easterly winds, these events have comparatively less effect on subsurface conditions. Despite their modest role in surface and subsurface warming, they resulted in high surface sublimation. Our estimated average sublimation rate of cDML for the five years is 0.17 mm per day, comparable to the rates estimated using AWS in eastern Dronning Maud Land (Van Den Broeke et al., 2004, 2009). During these events, the prevalent strong and dry winds increased sublimation to a mean rate of 0.27 mm per day.

4. Discussion

Accurate determination of ice sheet surface temperature is vital to understanding the impact of sudden atmospheric warming events on ice sheet surface energy balance, mass balance (through melting and sublimation) and subsurface temperature distribution. The temporal evolution of ISST is determined by the energy balance at the surface and near-surface air temperature is only one contributor to it. Hence direct examination of ISST provides a better picture of the impact of these events on the ice sheet surface rather than the 2 m air temperature measured by AWS. However, the direct measurement of ISST temperature is sparse over Antarctica. Satellite-derived land surface temperature is an excellent tool for studying ISST due to its large spatial coverage, however, it is limited to clear sky conditions. From our analysis, we see that borehole thermistors serve as a good tool for obtaining ice sheet surface and subsurface temperatures year-round in high temporal resolution. With proper consideration of annual accumulation over the region and burial of thermistors each year, the data can be extended to many years over any region in Antarctica.

The implementation of a thermistor string assembly offers notable advantages in terms of cost-effectiveness, maintenance simplicity, and straightforward installation procedures making it an adaptable complement to any ice core drilling program. Integration of satellite-based data transmission capabilities with these assemblies holds the

https://doi.org/10.5194/egusphere-2024-1666
Preprint. Discussion started: 11 June 2024

potential to establish a comprehensive network for continuous ISST monitoring. The acquired dataset can serve as a pivotal input for refining ice sheet and firn models, facilitating validation processes for both satellite-derived observations and model outputs. It is to be noted that the spacing between thermistors and accuracy in the estimation of accumulation rate over the region determines the accuracy of ISST measurements. Inaccurate estimation of precipitation and large spacing between thermistors might hinder the identification of the exact surface level and therefore produce deviations from the actual ISST.

In comparison with the skin temperature of ERA5, the borehole surface temperature had small amplitudes of day-to-day fluctuations, even though they followed a similar pattern as that of 2 m air temperature (Supplementary Figure 2s). This dampening of temperature fluctuations over the ice sheet surface compared to near-surface air is expected and borehole thermistors provided a more realistic behaviour of the ice sheet surface. In addition, the yearly mean values during 2015 were -24.43 °C and -25.15 °C for borehole and ERA5 surface temperatures respectively, indicating cold bias in ERA 5 skin temperature. We observe from our study that borehole thermistor measurements can be used to conduct a year-round study of ISST and accurately derive ground heat flux.

Our study suggests that the largest contributors to ice sheet surface and subsurface temperatures of cDML were warm air advection and cloud-induced longwave radiation associated with low-pressure systems. They resulted in T2m warming of 4.4-24.6 C and ISSW of 2-11.7 C and a deeper subsurface warming of the top 40-125 cm of firn. Our results revealed that the subsurface warming and maximum depth of penetration were more for ISSW events with surface easterly winds, indicating larger impacts on the microphysical properties of firn.

The ISST affects some important subsurface processes of ice sheets that determine the health of the firn layer. The warmer the subsurface temperatures, the faster the snow metamorphism and gravitational densification (Jordan et al., 2008; Ligtenberg et al., 2011). Warm ice is less viscous and therefore more prone to deformations (Weertman, 1983). When all other environmental parameters remain the same, the warm ice pack might lead to faster flow velocities. Warm surface and subsurface temperatures might alter the water retention and refreezing capacity of the firn layer by changing its microphysical properties (Courville et al., 2010; Albert and Shultz, 2002), leading to meltwater runoff and ponding. Hence, frequent occurrences of these events might warm the firn and eventually change its physical properties.

The southern ocean is a region of high storm activity at all times of year (Hoskins and Hodges, 2005) and has witnessed increased cyclone events due to global warming (Reboita et al., 2015). The increased cyclones in the southern hemisphere, irrespective of the season, could also influence these ISSW events over the cDML region. We observed atmospheric blocking of low-pressure systems for all the easterly wind events including the case study. This condition favoured prolonged warm air advection towards the region, an important factor for the extent (and duration) of ISSW. Damião Mendes and Cavalcanti, (2014) reported that atmospheric blocking days over the south Atlantic are maximum for winter and early spring. For the period 1979-2000, they observed that the frequency and duration of blocking events over the South Atlantic show large interannual variability with maximum during positive phases of Southern Annular Mode and El Nino years. Hence, these conditions might impact the ISSW extent and duration of cDML as well.

https://doi.org/10.5194/egusphere-2024-1666
Preprint. Discussion started: 11 June 2024

The ISSW associated with easterly wind events were attributed to enhanced LWD from clouds. The LWD from clouds depends on the cloud's optical thickness, liquid water path (LWP) and cloud phase (Wille et al., 2019; Bennartz et al., 2013; Nicolas et al., 2017). Changes in any of these parameters can alter the LWD and thereby the extent of warming. Kittel et al (2022) projected extensive melting of Antarctic ice shelves by increased liquid water in clouds via radiation perturbations. Therefore major uncertainty in surface warming is related to the increase of low-level liquid clouds which would emit more LWD leading to surface warming (Bennartz et al., 2013; Hofer et al., 2019; Gorodetskaya et al., 2015). A detailed study on the impact of frequent ISSW events over the physical properties of the firn layer might benefit in understanding the response of the ice sheet's interior to the changing climate.

The second category of ISSW over cDML was associated with increased turbulent heat flux from enhanced southeasterly winds blowing from the interior of the continent. From the case study, the origin of these warm and dry katabatic winds was from a warm air mass associated with a low-pressure system that recurved reaching high inland of the continent and descended eventually as enhanced katabatic winds to warm adiabatically before reaching the coast. Previously over the Indian Ocean sector of the Southern Ocean, similar recurving events have been observed as a result of an atmospheric river event resulting in an anomalous atmospheric warming of >14°C (Turner et al., 2022). This is the first time, recurved foehn winds have been reported in cDML in association with ISSW.

These events had modest ice sheet surface warming and shallow heat penetration depths even though they were observed with high T2m warming (4.9-15.8 C). This suggests that the impact of warming events on surface and subsurface temperatures depends on meteorological conditions and air temperature is only one contributor to it. Nevertheless, these events had a notable impact on the ice sheet surface through enhanced sublimation. Surface sublimation affects the mass balance of ice sheets by removing the precipitation (Barral et al., 2014; Grazioli et al., 2017) and altering the composition of ice cores (Masson-Delmotte et al., 2008).

It is noteworthy that we did not observe any melting near the borehole location due to subzero base temperatures in all seasons. However, considering the spatial extent of these warming episodes (Supplementary Figure 11s), surface melting could be induced by these events over the ice shelves during summer. There are studies on the melt layers captured in ice cores retrieved from coastal regions of Antarctica, including DML (Dey et al., 2022; Kaczmarska et al., 2006). Such melt layers cause changes in the physical and chemical properties of ice and affect their interpretation of past climate (Pohjola et al., 2002).

5. Conclusion

Using thermistors deployed in an ice core borehole, we examined the Ice sheet surface warming events of cDML during 2014-2018. The thermistor string assemblage provided an accurate estimation of ice sheet surface and subsurface temperatures over cDML. It recorded 70 major ISSW events, occurring in all seasons with a warming in the range of 2 – 11.7 °C.

The study identified two major meteorological conditions during ISSW, associated with surface easterly winds and precipitation and surface south easterly winds without precipitation. Although the air temperature warmed in the same range for both cases (~ 4 – 20 °C), the former had more effect on the ice sheet surface and subsurface temperatures. Occurring 85% of the time during the study period, these events resulted in an ISSW of 2-11.7 °C with

https://doi.org/10.5194/egusphere-2024-1666
Preprint. Discussion started: 11 June 2024

a lag of 2 days from T2m and deeper subsurface heat penetration up to 40-125 cm. For the study period, the largest difference between T2m and ISST occurred during autumn and the least during summer and spring. They were driven by warm air advection and enhanced cloud-induced downward longwave radiation associated with low-pressure systems over the region. We observed an average of 12 events per year with maximum occurrence in winter and spring. Further monitoring of these events is important over the study region since it has the greatest impact on the ice sheet surface and subsurface.

The second type of warming events associated with surface easterly winds occurred due to a relatively less studied phenomenon of recurved foehn winds. We report the first multi-year study of these events in cDML and examine their mechanism of warming. They warmed the surface directly via turbulent heat transfer from strong and adiabatically warm winds from the interior. Although warmed the T2m significantly, they had modest effects on the ice sheet surface and subsurface temperatures but resulted in significant sublimation of surface snow over the region.

Our study suggests that the impact of atmospheric warming over ice sheet surface and subsurface temperatures depends on the mechanism of warming and meteorological conditions. The frequency and duration of such events are important for the surface and sub-surface processes of ice sheets.

Data availability

The data used in this work is available at http://ramadda.npdc.ncpor.res.in/repository/entry/show?entryid=a9bcd8a3-7417-4bad-bd1e-44ecf1b8ad69. It includes the six hourly dataset of borehole thermistor measurements from cDML for 2014-2018 from a height of 1.2m to a depth of 30m. ERA5 data can be downloaded from the Copernicus Climate Data store provided by ECMWF (https://doi.org/10.24381/cds.f17050d7, Hersbach et al., 2020). RACMO2.3p2 model output is obtained from the Zenodo data repository on a monthly scale with a spatial resolution of 27 km (DOI 10.5281/zenodo.7760490, van Wessem et al., 2023). The daily SEB fluxes from an AWS in Roi Baudouin Ice Shelf is available on PANGEA database (https://doi.org/10.1594/PANGAEA.910473, (Jakobs et al., 2020b, a)) Novolazarskaya station observation is collected as part of READER project and is available on ftp://ftp.bas.ac.uk/src/ANTARCTIC_METEOROLOGICAL_DATA/GTS_DATA/SURFACE/ (Turner et al., 2004).

Author contribution

E M Gayathri: Conceptualization, Methodology, Data Curation, Formal analysis, Writing - Original Draft. **C M Laluraj:** Conceptualization, Methodology, Writing - Review & Editing, **K Satheesan:** Validation, Writing – Review & Editing. **Kenichi Matsuoka:** Supervision, Conceptualization, Review & Editing, **Mahalinganathan Kandanathan:** Data collection, **Meloth Thamban:** Project administration.

Competing interests

The authors do not have any competing interests.

Acknowledgements

https://doi.org/10.5194/egusphere-2024-1666
Preprint. Discussion started: 11 June 2024

We thank the Director, National Centre for Polar and Ocean Research and Ministry of Earth Sciences (MOES), India for financial support through the project 'PACER - Cryosphere and Climate'. We sincerely thank Dr. John Turner, formerly of British Antarctic Survey (BAS), for proofreading this version and sharing his valuable comments. We also express our gratitude to Mr. Bhikaji L Redkar for deploying the instrument in the field. This is NCPOR contribution No. xxx.

References

Albert, M. R. and Shultz, E. F.: Snow and firn properties and air–snow transport processes at Summit, Greenland, Atmos. Environ., 36, 2789–2797, 2002.

Amory, C., Buizert, C., Buzzard, S., Case, E., Clerx, N., Culberg, R., Datta, R. T., Dey, R., Drews, R., Dunmire, D., Eayrs, C., Hansen, N., Humbert, A., Kaitheri, A., Keegan, K., Kuipers Munneke, P., Lenaerts, J. T. M., Lhermitte, S., Mair, D., McDowell, I., Mejia, J., Meyer, C. R., Morris, E., Moser, D., Oraschewski, F. M., Pearce, E., de Roda Husman, S., Schlegel, N.-J., Schultz, T., Simonsen, S. B., Stevens, C. M., Thomas, E. R., Thompson-Munson, M., Wever, N., Wouters, B., and team, T. F. S.: Firn on ice sheets, Nat. Rev. Earth Environ., 5, 79–99, https://doi.org/10.1038/s43017-023-00507-9, 2024.

Argentini, S., Pietroni, I., Mastrantonio, G., Viola, A. P., Dargaud, G., and Petenko, I.: Observations of near surface wind speed, temperature and radiative budget at Dome C, Antarctic Plateau during 2005, Antarct. Sci., 26, 104–112, https://doi.org/10.1017/S0954102013000382, 2014.

Arthur, J. F., Stokes, C. R., Jamieson, S. S. R., Carr, J. R., and Leeson, A. A.: Distribution and seasonal evolution of supraglacial lakes on Shackleton Ice Shelf, East Antarctica, Cryosph., 14, 4103–4120, 2020.

Barral, H., Genthon, C., Trouvilliez, A., Brun, C., and Amory, C.: Blowing snow in coastal Adélie Land, Antarctica: three atmospheric-moisture issues, Cryosph., 8, 1905–1919, 2014.

Bennartz, R., Shupe, M. D., Turner, D. D., Walden, V. P., Steffen, K., Cox, C. J., Kulie, M. S., Miller, N. B., and Pettersen, C.: July 2012 Greenland melt extent enhanced by low-level liquid clouds, Nature, 496, 83–86, 2013.

Bliss, A. K., Cuffey, K. M., and Kavanaugh, J. L.: Sublimation and surface energy budget of Taylor Glacier, Antarctica, J. Glaciol., 57, 684–696, https://doi.org/10.3189/002214311797409767, 2011.

Bozkurt, D., Rondanelli, R., Marín, J. C., and Garreaud, R.: Foehn Event Triggered by an Atmospheric River Underlies Record-Setting Temperature Along Continental Antarctica, J. Geophys. Res. Atmos., 123, 3871–3892, https://doi.org/10.1002/2017JD027796, 2018.

Brandt, R. E. and Warren, S. G.: Solar-heating rates and temperature profiles in Antarctic snow and ice, J. Glaciol.,

https://doi.org/10.5194/egusphere-2024-1666
Preprint. Discussion started: 11 June 2024

39, 99–110, https://doi.org/10.3189/S0022143000015756, 1993.

Van Den Broeke, M. R., Reijmer, C. H., and Van De Wal, R. S. W.: A study of the surface mass balance in Dronning Maud Land, Antarctica, using automatic weather stationS, 2004.

Van Den Broeke, M., König-Langlo, G., Picard, G., Kuipers Munneke, P., and Lenaerts, J.: Surface energy balance, melt and sublimation at Neumayer Station, East Antarctica, Antarct. Sci., 22, 87–96, https://doi.org/10.1017/S0954102009990538, 2009.

Bromwich, D. H.: Satellite Analyses of Antarctic Katabatic Wind Behavior, Bull. Am. Meteorol. Soc., 70, 738–749, https://doi.org/10.1175/1520-0477(1989)070<0738:SAOAKW>2.0.CO;2, 1989.

Bromwich, D. H., Carrasco, J. F., Zhong Liu, and Ren-Yow Tzeng: Hemispheric atmospheric variations and oceanographic impacts associated with katabatic surges across the Ross ice shelf, Antarctica, J. Geophys. Res. Atmos., 98, 13045–13062, https://doi.org/10.1029/93JD00562, 1993.

Cape, M. R., Vernet, M., Skvarca, P., Marinsek, S., Scambos, T., and Domack, E.: Foehn winds link climate-driven warming to ice shelf evolution in Antarctica, J. Geophys. Res. Atmos., 120, 11,037-11,057, https://doi.org/10.1002/2015JD023465, 2015.

Chouksey, A., Thakur, P. K., Sahni, G., Swain, A. K., Aggarwal, S. P., and Kumar, A. S.: Mapping and identification of ice-sheet and glacier features using optical and SAR data in parts of central Dronning Maud Land (cDML), East Antarctica, Polar Sci., 30, 100740, https://doi.org/https://doi.org/10.1016/j.polar.2021.100740, 2021.

Courville, Z., Hörhold, M., Hopkins, M., and Albert, M.: Lattice-Boltzmann modeling of the air permeability of polar firn, J. Geophys. Res. Earth Surf., 115, 2010.

Damião Mendes, M. C. and Cavalcanti, I. F. A.: The relationship between the Antarctic oscillation and blocking events over the South Pacific and Atlantic Oceans, Int. J. Climatol., 34, 529–544, 2014.

Dell, R., Arnold, N., Willis, I., Banwell, A., Williamson, A., Pritchard, H., and Orr, A.: Lateral meltwater transfer across an Antarctic ice shelf, Cryosph., 14, 2313–2330, 2020.

Dey, R., Thamban, M., Laluraj, C. M., Mahalinganathan, K., Redkar, B. L., Kumar, S., and Matsuoka, K.: Application of visual stratigraphy from line-scan images to constrain chronology and melt features of a firn core from coastal Antarctica, J. Glaciol., 1–12, https://doi.org/10.1017/JOG.2022.59, 2022.

Emanuelsson, B. D., Bertler, N. A. N., Neff, P. D., Renwick, J. A., Markle, B. R., Baisden, W. T., and Keller, E. D.: The role of Amundsen–Bellingshausen Sea anticyclonic circulation in forcing marine air intrusions into West Antarctica, Clim. Dyn., 51, 3579–3596, https://doi.org/10.1007/S00382-018-4097-3/FIGURES/10, 2018.

https://doi.org/10.5194/egusphere-2024-1666
Preprint. Discussion started: 11 June 2024

Feron, S., Cordero, R. R., Damiani, A., Malhotra, A., Seckmeyer, G., and Llanillo, P.: Warming events projected to become more frequent and last longer across Antarctica, Sci. Rep., 11, 1–9, https://doi.org/10.1038/s41598-021-98619-z, 2021.

Firn Symposium Team, Amory, C., Buizert, C., Buzzard, S., Case, E., Clerx, N., Culberg, R., Datta, R. T., Dey, R., Drews, R., Dunmire, D., Eayrs, C., Hansen, N., Humbert, A., Kaitheri, A., Keegan, K., Kuipers Munneke, P., Lenaerts, J. T. ~M., Lhermitte, S., Mair, D., McDowell, I., Mejia, J., Meyer, C. R., Morris, E., Moser, D., Oraschewski, F. M., Pearce, E., de Roda Husman, S., Schlegel, N.-J., Schultz, T., Simonsen, S. B., Stevens, C. M., Thomas, E. R., Thompson-Munson, M., Wever, N., and Wouters, B.: Firn on ice sheets, Nat. Rev. Earth Environ., 5, 79–99, https://doi.org/10.1038/s43017-023-00507-9, 2024.

Garza-Giron, R. and Tulaczyk, S. M.: Brief communication: Significant cold bias in ERA5 output for McMurdo region, Antarctica, Cryosph. Discuss., 2023, 1–10, https://doi.org/10.5194/tc-2023-44, 2023.

Ghiz, M. L., Scott, R. C., Vogelmann, A. M., Lenaerts, J. T. M., Lazzara, M., and Lubin, D.: Energetics of surface melt in West Antarctica, Cryosphere, 15, 3459–3494, https://doi.org/10.5194/TC-15-3459-2021, 2021.

Goel, V., Matsuoka, K., Berger, C. D., Lee, I., Dall, J., and Forsberg, R.: Characteristics of ice rises and ice rumples in Dronning Maud Land and Enderby Land, Antarctica, J. Glaciol., 66, 1064–1078, https://doi.org/DOI: 10.1017/jog.2020.77, 2020.

González-Herrero, S., Barriopedro, D., Trigo, R. M., López-Bustins, J. A., and Oliva, M.: Climate warming amplified the 2020 record-breaking heatwave in the Antarctic Peninsula, Commun. Earth Environ., 3, 1–9, https://doi.org/10.1038/s43247-022-00450-5, 2022.

Gorodetskaya, I. V, Kneifel, S., Maahn, M., Van Tricht, K., Thiery, W., Schween, J. H., Mangold, A., Crewell, S., and Van Lipzig, N. P. M.: Cloud and precipitation properties from ground-based remote-sensing instruments in East Antarctica, Cryosph., 9, 285–304, 2015.

Grazioli, J., Madeleine, J. B., Gallée, H., Forbes, R. M., Genthon, C., Krinner, G., and Berne, A.: Katabatic winds diminish precipitation contribution to the Antarctic ice mass balance, Proc. Natl. Acad. Sci. U. S. A., 114, 10858–10863, https://doi.org/10.1073/PNAS.1707633114/SUPPL_FILE/PNAS.201707633SI.PDF, 2017.

Heinemann, G.: On the streakiness of katabatic wind signatures on high-resolution AVHRR satellite images: Results from the aircraft-based experiment KABEG, Polarforschung, 66, 19–30, 2000.

Hersbach, H., Bell, B., Berrisford, P., Hirahara, S., Horányi, A., Muñoz-Sabater, J., Nicolas, J., Peubey, C., Radu, R., Schepers, D., Simmons, A., Soci, C., Abdalla, S., Abellan, X., Balsamo, G., Bechtold, P., Biavati, G., Bidlot, J., Bonavita, M., De Chiara, G., Dahlgren, P., Dee, D., Diamantakis, M., Dragani, R., Flemming, J., Forbes, R., Fuentes, M., Geer, A., Haimberger, L., Healy, S., Hogan, R. J., Hólm, E., Janisková, M., Keeley, S., Laloyaux, P.,

https://doi.org/10.5194/egusphere-2024-1666
Preprint. Discussion started: 11 June 2024

Lopez, P., Lupu, C., Radnoti, G., de Rosnay, P., Rozum, I., Vamborg, F., Villaume, S., and Thépaut, J. N.: The ERA5 global reanalysis, Q. J. R. Meteorol. Soc., 146, 1999–2049, https://doi.org/10.1002/qj.3803, 2020.

Hirasawa, N., Nakamura, H., and Yamanouchi, T.: Abrupt changes in meteorological conditions observed at an inland Antarctic Station in association with wintertime blocking, Geophys. Res. Lett., 27, 1911–1914, https://doi.org/10.1029/1999GL011039, 2000.

Hofer, S., Tedstone, A. J., Fettweis, X., and Bamber, J. L.: Cloud microphysics and circulation anomalies control differences in future Greenland melt, Nat. Clim. Chang., 9, 523–528, 2019.

Hogan, A.: A synthesis of warm air advection to the South Polar Plateau, J. Geophys. Res. Atmos., 102, 14009–14020, 1997.

Hui, F., Ci, T., Cheng, X., Scambo, T. A., Liu, Y., Zhang, Y., Chi, Z., Huang, H., Wang, X., and Wang, F.: Mapping blue-ice areas in Antarctica using ETM+ and MODIS data, Ann. Glaciol., 55, 129–137, 2014.

Jakobs, C. L., Reijmer, C. H., Smeets, C. J. P. P., Trusel, L. D., van Wessem, J. M., van de Berg, W. J., and van den Broeke, M. R.: A benchmark dataset of in situ Antarctic surface melt rates and energy balance, J. Glaciol., 66, 291–302, https://doi.org/DOI: 10.1017/jog.2020.6, 2020a.

Jakobs, C. L., Reijmer, C. H., van den Broeke, M. R., Smeets, P., and König-Langlo, G.: High-resolution meteorological observations, Surface Energy Balance components and miscellaneous data from 10 AWS and one staffed station in Antarctica, https://doi.org/10.1594/PANGAEA.910473, 8 January 2020b.

Jordan, R. E., Albert, M. R., and Brun, E.: Snow and Climate: Physical Processes within the snow cover and their parametrization, 2008.

Kaczmarska, M., Isaksson, E., Karlöf, L., Brandt, O., Winther, J. G., Van De Wal, R. S. W., Van Den Broeke, M., and Johnsen, S. J.: Ice core melt features in relation to Antarctic coastal climate, Antarct. Sci., 18, 271–278, https://doi.org/10.1017/S0954102006000319, 2006.

King, J. C., Gadian, A., Kirchgaessner, A., Kuipers Munneke, P., Lachlan-Cope, T. A., Orr, A., Reijmer, C., Van Den Broeke, M. R., Van Wessem, J. M., and Weeks, M.: Validation of the summertime surface energy budget of Larsen C Ice Shelf (Antarctica) as represented in three high-resolution atmospheric models, J. Geophys. Res. Atmos., 120, 1335–1347, 2015.

King, J. C., Kirchgaessner, A., Bevan, S., Elvidge, A. D., Kuipers Munneke, P., Luckman, A., Orr, A., Renfrew, I. A., and van den Broeke, M. R.: The Impact of Föhn Winds on Surface Energy Balance During the 2010–2011 Melt Season Over Larsen C Ice Shelf, Antarctica, J. Geophys. Res. Atmos., 122, 12,062-12,076, https://doi.org/10.1002/2017JD026809, 2017.

https://doi.org/10.5194/egusphere-2024-1666
Preprint. Discussion started: 11 June 2024

Kittel, C., Amory, C., Hofer, S., Agosta, C., Jourdain, N. C., Gilbert, E., Le Toumelin, L., Vignon, É., Gallée, H., and Fettweis, X.: Clouds drive differences in future surface melt over the Antarctic ice shelves, Cryosph., 16, 2655–2669, https://doi.org/10.5194/tc-16-2655-2022, 2022.

Lenaerts, J. T. M., Lhermitte, S., Drews, R., Ligtenberg, S. R. M., Berger, S., Helm, V., Smeets, C. J. P. P., Broeke, M. R. V. Den, Van De Berg, W. J., Van Meijgaard, E., Eijkelboom, M., Eisen, O., and Pattyn, F.: Meltwater produced by wind–albedo interaction stored in an East Antarctic ice shelf, Nat. Clim. Chang., 7, 58–62, https://doi.org/10.1038/nclimate3180, 2017.

Ligtenberg, S. R. M., Helsen, M. M., and Van den Broeke, M. R.: An improved semi-empirical model for the densification of Antarctic firn, Cryosph., 5, 809–819, 2011.

Van Lipzig, N. P. M., Turner, J., Colwell, S. R., and van Den Broeke, M. R.: The near-surface wind field over the Antarctic continent, Int. J. Climatol. A J. R. Meteorol. Soc., 24, 1973–1982, 2004.

Liston, G. E., Winther, J. G., Bruland, O., Elvehøy, H., and Sand, K.: Below-surface ice melt on the coastal Antarctic ice sheet, J. Glaciol., 45, 273–285, https://doi.org/10.3189/s0022143000001775, 1999.

de Los Milagros Skansi, M., King, J., Lazzara, M. A., Cerveny, R. S., Stella, J. L., Solomon, S., Jones, P., Bromwich, D., Renwick, J., and Burt, C. C.: Evaluating the highest temperature extremes in the Antarctic, Eos (Washington. DC)., 98, 18–23, 2017.

Massom, R. A., Pook, M. J., Comiso, J. C., Adams, N., Turner, J., Lachlan-Cope, T., and Gibson, T. T.: Precipitation over the interior East Antarctic ice sheet related to midlatitude blocking-high activity, J. Clim., 17, 1914–1928, 2004.

Masson-Delmotte, V., Hou, S., Ekaykin, A., Jouzel, J., Aristarain, A., Bernardo, R. T., Bromwich, D., Cattani, O., Delmotte, M. M., Falourd, S., Frezzotti, M., Gallée, H., Genoni, L., Isaksson, E., Landais, A., Helsen, M. M., Hoffmann, G., Lopez, J., Morgan, V., Motoyama, H., Noone, D., Oerter, H., Petit, J. R., Royer, A., Uemura, R., Schmidt, G. A., Schlosser, E., Simões, J. C., Steig, E. J., Stenni, B., Stievenard, M., Van Den Broeke, M. R., Van De Wal, R. S. W., Van De Berg, W. J., Vimeux, F., and White, J. W. C.: A Review of Antarctic Surface Snow Isotopic Composition: Observations, Atmospheric Circulation, and Isotopic Modeling, J. Clim., 21, 3359–3387, https://doi.org/10.1175/2007JCLI2139.1, 2008.

Matsuoka, K., Hindmarsh, R. C. A., Moholdt, G., Bentley, M. J., Pritchard, H. D., Brown, J., Conway, H., Drews, R., Durand, G., Goldberg, D., Hattermann, T., Kingslake, J., Lenaerts, J. T. M., Martín, C., Mulvaney, R., Nicholls, K. W., Pattyn, F., Ross, N., Scambos, T., and Whitehouse, P. L.: Antarctic ice rises and rumples: Their properties and significance for ice-sheet dynamics and evolution, Earth-Science Rev., 150, 724–745, https://doi.org/https://doi.org/10.1016/j.earscirev.2015.09.004, 2015.

https://doi.org/10.5194/egusphere-2024-1666
Preprint. Discussion started: 11 June 2024

McDowell, I. E., Albert, M. R., Lieblappen, S. A., and Keegan, K. M.: Local Weather Conditions Create Structural Differences between Shallow Firn Columns at Summit, Greenland and WAIS Divide, Antarctica, Atmosphere (Basel)., 11, https://doi.org/10.3390/atmos11121370, 2020.

Moussavi, M., Pope, A., Halberstadt, A. R. W., Trusel, L. D., Cioffi, L., and Abdalati, W.: Antarctic supraglacial lake detection using Landsat 8 and Sentinel-2 imagery: Towards continental generation of lake volumes, Remote Sens., 12, 134, 2020.

Nicolas, J. P. and Bromwich, D. H.: Climate of West Antarctica and Influence of Marine Air Intrusions, J. Clim., 24, 49–67, https://doi.org/10.1175/2010JCLI3522.1, 2011.

Nicolas, J. P., Vogelmann, A. M., Scott, R. C., Wilson, A. B., Cadeddu, M. P., Bromwich, D. H., Verlinde, J., Lubin, D., Russell, L. M., Jenkinson, C., Powers, H. H., Ryczek, M., Stone, G., and Wille, J. D.: January 2016 extensive summer melt in West Antarctica favoured by strong El Niño, Nat. Commun., 8, 1–10, https://doi.org/10.1038/ncomms15799, 2017.

Nielsen-Englyst, P., Høyer, J. L., Madsen, K. S., Tonboe, R., Dybkjær, G., and Alerskans, E.: In situ observed relationships between snow and ice surface skin temperatures and 2 m air temperatures in the Arctic, Cryosph., 13, 1005–1024, 2019.

Nielsen, E. B., Katurji, M., Zawar-Reza, P., and Meyer, H.: Antarctic daily mesoscale air temperature dataset derived from MODIS land and ice surface temperature, Sci. Data, 10, 833, https://doi.org/10.1038/s41597-023-02720-z, 2023.

Noël, B., Van De Berg, W. J., Van Wessem, J. M., Van Meijgaard, E., Van As, Di., Lenaerts, J., Lhermitte, S., Kuipers Munneke, P., Smeets, C. J. P., and Van Ulft, L. H.: Modelling the climate and surface mass balance of polar ice sheets using RACMO2–Part 1: Greenland (1958–2016), Cryosph., 12, 811–831, 2018.

Noone, D., Turner, J., and Mulvaney, R.: Atmospheric signals and characteristics of accumulation in Dronning Maud Land, Antarctica, J. Geophys. Res. Atmos., 104, 19191–19211, 1999.

Östin, R. and Andersson, S.: Frost growth parameters in a forced air stream, Int. J. Heat Mass Transf., 34, 1009–1017, https://doi.org/10.1016/0017-9310(91)90012-4, 1991.

Parish, T. R. and Bromwich, D. H.: Reexamination of the near-surface airflow over the Antarctic continent and implications on atmospheric circulations at high southern latitudes, Mon. Weather Rev., 135, 1961–1973, 2007.

Pohjola, V., Moore, J., Isaksson, E., Jauhiainen, T., Martma, T., Meijer, H. A. J., Vaikmäe, R., and Van de Wal, R. S. W.: An ice core record from Lomonsovfonna, Svalbard: investigation of depositional signals with respect to melt, J. Geophys. Res., 10, 2002.

https://doi.org/10.5194/egusphere-2024-1666
Preprint. Discussion started: 11 June 2024

Rott, H., Skvarca, P., and Nagler, T.: Rapid Collapse of Northern Larsen Ice Shelf, Antarctica, Science (80-.)., 271, 788–792, https://doi.org/10.1126/SCIENCE.271.5250.788, 1996.

Sato, K. and Simmonds, I.: Antarctic skin temperature warming related to enhanced downward longwave radiation associated with increased atmospheric advection of moisture and temperature, Environ. Res. Lett., 16, 064059, https://doi.org/10.1088/1748-9326/AC0211, 2021.

Scambos, T. A., Bohlander, J. A., Shuman, C. A., and Skvarca, P.: Glacier acceleration and thinning after ice shelf collapse in the Larsen B embayment, Antarctica, Geophys. Res. Lett., 31, 18402, https://doi.org/10.1029/2004GL020670, 2004.

Schlosser, E., Manning, K. W., Powers, J. G., Duda, M. G., Birnbaum, G., and Fujita, K.: Characteristics of high-precipitation events in Dronning Maud Land, Antarctica, J. Geophys. Res. Atmos., 115, https://doi.org/10.1029/2009JD013410, 2010.

Schlosser, E., Stenni, B., Valt, M., Cagnati, A., Powers, J. G., Manning, K. W., Raphael, M., and Duda, M. G.: Precipitation and synoptic regime in two extreme years 2009 and 2010 at Dome C, Antarctica–implications for ice core interpretation, Atmos. Chem. Phys., 16, 4757–4770, 2016.

Shepherd, A., Ivins, E., Rignot, E., Smith, B., van den Broeke, M., Velicogna, I., Whitehouse, P., Briggs, K., Joughin, I., and Krinner, G.: Mass balance of the Antarctic Ice Sheet from 1992 to 2017. Nature, 2018.

Silber, I., Verlinde, J., Wang, S. H., Bromwich, D. H., Fridlind, A. M., Cadeddu, M., Eloranta, E. W., and Flynn, C. J.: Cloud influence on ERA5 and AMPS surface downwelling longwave radiation biases in West Antarctica, J. Clim., 32, 7935–7949, https://doi.org/10.1175/JCLI-D-19-0149.1, 2019.

Sinclair, M. R.: Record-high temperatures in the Antarctic—A synoptic case study, Mon. Weather Rev, 109, 2234–2242, 1981.

Spaulding, N. E., Meese, D. A., and Baker, I.: Advanced microstructural characterization of four East Antarctic firn/ice cores, J. Glaciol., 57, 796–810, 2011.

Speirs, J. C., Steinhoff, D. F., McGowan, H. A., Bromwich, D. H., and Monaghan, A. J.: Foehn Winds in the McMurdo Dry Valleys, Antarctica: The Origin of Extreme Warming Events, J. Clim., 23, 3577–3598, https://doi.org/10.1175/2010JCLI3382.1, 2010.

Stokes, C. R., Sanderson, J. E., Miles, B. W. J., Jamieson, S. S. R., and Leeson, A. A.: Widespread distribution of supraglacial lakes around the margin of the East Antarctic Ice Sheet, Sci. Rep., 9, 1–14, https://doi.org/10.1038/s41598-019-50343-5, 2019.

Tetzner, D., Thomas, E., and Allen, C.: A validation of ERA5 reanalysis data in the southern antarctic peninsula—

https://doi.org/10.5194/egusphere-2024-1666
Preprint. Discussion started: 11 June 2024

Ellsworth land region, and its implications for ice core studies, Geosci., 9, https://doi.org/10.3390/geosciences9070289, 2019.

Tjernström, M., Shupe, M. D., Brooks, I. M., Persson, P. O. G., Prytherch, J., Salisbury, D. J., Sedlar, J., Achtert, P., Brooks, B. J., Johnston, P. E., Sotiropoulou, G., and Wolfe, D.: Warm-air advection, air mass transformation and fog causes rapid ice melt, Geophys. Res. Lett., 42, 5594–5602, https://doi.org/10.1002/2015GL064373, 2015.

Trabant, D. C. and Mayo, L. R.: Estimation and effects of internal accumulation on five glaciers in Alaska, Ann. Glaciol., 6, 113–117, 1985.

Turner, J., Colwell, S. R., Marshall, G. J., Lachlan-Cope, T. A., Carleton, A. M., Jones, P. D., Lagun, V., Reid, P. A., and Iagovkina, S.: The SCAR READER Project: Toward a High-Quality Database of Mean Antarctic Meteorological Observations, J. Clim., 17, 2890–2898, https://doi.org/https://doi.org/10.1175/1520-0442(2004)017<2890:TSRPTA>2.0.CO;2, 2004.

Turner, J., Phillips, T., Thamban, M., Rahaman, W., Marshall, G. J., Wille, J. D., Favier, V., Holly, V., Winton, L., Thomas, E., Wang, Z., Van Den Broeke, M., Hosking, J. S., and Lachlan-Cope, T.: The Dominant Role of Extreme Precipitation Events in Antarctic Snowfall Variability, Geophys. Res. Lett., 46, 3502–3511, https://doi.org/10.1029/2018GL081517, 2019.

Turner, J., Lu, H., King, J., Marshall, G. J., Phillips, T., Bannister, D., and Colwell, S.: Extreme temperatures in the Antarctic, J. Clim., 34, 2653–2668, https://doi.org/10.1175/JCLI-D-20-0538.1, 2021.

Turner, J., Lu, H., King, J. C., Carpentier, S., Lazzara, M., Phillips, T., and Wille, J.: An Extreme High Temperature Event in Coastal East Antarctica Associated With an Atmospheric River and Record Summer Downslope Winds, Geophys. Res. Lett., 49, 1–11, https://doi.org/10.1029/2021GL097108, 2022.

Vihma, T., Tuovinen, E., and Savijärvi, H.: Interaction of katabatic winds and near-surface temperatures in the Antarctic, 116, 21119, https://doi.org/10.1029/2010JD014917, 2011.

Weertman, J.: Creep deformation of ice, Annu. Rev. Earth Planet. Sci., 11, 215–240, 1983.

Wei, T., Yan, Q., and Ding, M.: Distribution and temporal trends of temperature extremes over Antarctica, Environ. Res. Lett., 14, https://doi.org/10.1088/1748-9326/ab33c1, 2019.

van Wessem, J. M., van de Berg, W. J., Noël, B. P. Y., van Meijgaard, E., Amory, C., Birnbaum, G., Jakobs, C. L., Krüger, K., Lenaerts, J. T. M., Lhermitte, S., Ligtenberg, S. R. M., Medley, B., Reijmer, C. H., van Tricht, K., Trusel, L. D., van Ulft, L. H., Wouters, B., Wuite, J., and van den Broeke, M. R.: Modelling the climate and surface mass balance of polar ice sheets using RACMO2 -- Part 2: Antarctica (1979--2016), Cryosph., 12, 1479–1498, https://doi.org/10.5194/tc-12-1479-2018, 2018.

https://doi.org/10.5194/egusphere-2024-1666
Preprint. Discussion started: 11 June 2024

van Wessem, J. M., van de Berg, W. J., and van den Broeke, M. R.: Data set: Monthly averaged RACMO2.3p2 variables; Antarctica, https://doi.org/10.5281/zenodo.7760491, March 2023.

Wille, J. D., Favier, V., Dufour, A., Gorodetskaya, I. V., Turner, J., Agosta, C., and Codron, F.: West Antarctic surface melt triggered by atmospheric rivers, Nat. Geosci., 12, 911–916, https://doi.org/10.1038/s41561-019-0460-1, 2019.

Zhu, J., Xie, A., Qin, X., Wang, Y., Xu, B., and Wang, Y.: An assessment of ERA5 reanalysis for antarctic near-surface air temperature, Atmosphere (Basel)., 12, https://doi.org/10.3390/atmos12020217, 2021.

Zou, X., Bromwich, D. H., Montenegro, A., Wang, S. H., and Bai, L.: Major surface melting over the Ross Ice Shelf part I: Foehn effect, Q. J. R. Meteorol. Soc., 147, 2874–2894, https://doi.org/10.1002/QJ.4104, 2021a.

Zou, X., Bromwich, D. H., Montenegro, A., Wang, S. H., and Bai, L.: Major surface melting over the Ross Ice Shelf part II: Surface energy balance, Q. J. R. Meteorol. Soc., 147, 2895–2916, https://doi.org/10.1002/QJ.4105, 2021b.